Responses to the reviewers

Title: Role of ammonia on fine-particle pH in agricultural regions of China: Comparison between urban and rural sites.

General Comments:

This manuscript presents simultaneous measurements of inorganic aerosol composition and key gas-phase species (NH3, HCl, HNO3) at two urban and three rural sites in Henan Province, China. The measurements occurred during the winter and capture one of the well-documented winter haze episodes. The focus of the manuscript is modeling aerosol pH at the urban-rural sites, and performing sensitivity tests to characterize the factors that most control pH during such polluted conditions. This is a novel and valuable data set that can add important insight to our understanding of aerosol pH. The topic is appropriate for ACP and will be of interest to a broad audience. The manuscript organization and figure quality are generally good, however certain elements of the presentation – namely the English usage – require improvements throughout to bring it up to publication quality. Several analyses and/or results require clarification, and a number of key references are missing. These comments are detailed below.

Thank you for your careful reading of our paper and valuable comments and suggestions. We believe that we have adequately addressed your comments. To facilitate your review, we used yellow highlights for your comments, and red color indicating our own corrections in the manuscript.

Specific Comments:

Missing from the manuscript is a discussion of measurement uncertainty and statistical significance of the various analyses. For example, throughout the manuscript (line 27–78, 194–195, 203–204, 228–229, 250–254, 260–261) concentrations or values at the five sites are compared and ranked. In some cases, the differences appear to be quite small, and are not likely statistically significant if uncertainty and measurement variability are taken into account.

Response: Thanks for the comment. We have added the uncertainty of each instrument based on references or instrument manuals (line 128–146), and pH uncertainty was evaluated by calculating the input data in two extreme scenarios (see Section 2.4). Considering the measurement uncertainty and statistical significance, we have modified the comparison between urban and rural sites instead of the rank of five sites in the revised version (line 248–250, 254–256, 369–371).

Figures 5, 6, and 7 and the associated discussion in Section 3.3 need clarification. It is not clear how the different sensitivity analyses were performed (What was held constant? What was varied? Which conditions were used for the base simulations?). In some cases, the interpretations also require clarification: e.g., the authors use "%RSD" – how is this actually defined? It seems in the text that they interpret %RSD as actual pH values instead of a percentage, but this could just reinforce the point that this discussion needs to be improved. On the point of RSD, the description in the text does not seem consistent with what is plotted in Fig. 5 or Fig. 7.

Response: Sorry for the misunderstanding. We have added a paragraph to describe the sensitivity tests and explain the use of RSD (line 276–290, 310–315): "To explore the dominant factors that determine the local particle pH level and resulting in the high pH at rural sites, sensitivity tests of pH to chemical species (i.e., TNH_x, TH_2SO_4, TNO_3, TCl, TNa, K^+, Ca^{2+}, and Mg^{2+}) and meteorological parameters (i.e., T and RH) were performed. Firstly, the real-time measured values of a variable (e.g., TNH_x) and average values of other parameters (i.e., TH_2SO_4, TNO_3, TCl, TNa, K^+, Ca^{2+}, Mg^{2+}, T and RH) during Case 2 were input into ISORROPIA-II to investigate the sensitivity of local pH to this variable (i.e., TNH_x) (Ding et al., 2019), and results are listed in Table 4 and Fig. S10. In addition, a given range for a variable for all sites with corresponding average values of other parameters was simulated to compare its effects on pH among five sites (Figs. 5 and S11). The chosen variation range for each variable was close to the observed minimum and maximum values (Table S4), which aims to better reflect the actual observation conditions. The degree of sensitivity was represented as the relative standard deviation (%RSD) of the re-calculated pH values. RSD calculates the absolute value of the coefficient of variation, which helps us to determine how small or large is the standard deviation when compared to the mean of the re-calculated pH data set. Therefore, when the re-calculated pH data set has a higher RSD value, this variable can change the pH easier and is more important for local pH."

As stated above, the manuscript requires editing for grammar, English usage, and punctuation. Since this is an issue throughout the manuscript, specific areas for improvement are not identified in ‘Technical Corrections’.

Response: We have sought a professional expert to edit our revised manuscript for better flow and readability as well as for correcting some grammatical and editorial errors. In addition, this paper has been re-checked using a professional language editing service (Essaystar Group), Editing Certificate will be provided upon request. Hope it has been improved by correcting the English usage in the revised version.

A number of key references are missing. These need to be cited and the discussion enhanced to include the context they provide. To Sections 3.3 and 3.4 add discussion of Weber et al. (2016), Vasilakos et al. (2018), and Nenes et al. (2019). On the meteorological effects on pH, add discussion of Battaglia et al. (2017) and Tao and Murphy (2019). For recent discussions of aerosol pH importance, definitions, and reported ambient levels, add discussion of Pye et al. (2019). Line 67 refers to several other studies that have examined aerosol pH in agricultural regions of China – the present results should be contrasted with these prior studies.

Response: Thanks. We have cited the above-mentioned papers and enhanced the discussion in Sections 3.3 and 3.4. (Line 57–59, 70–73, 82–83, 292–297, 303–306)

Original line 67 (line 80 in the revised version) refers to nearly none of the studies that have examined aerosol pH in agricultural regions of China. In fact, until now, we do not have found a paper focused on the $PM_{2.5}$ acidity in agricultural regions of China. Moreover, we add the discussion about the difference of pH at rural sites between the present results and previous studies in the USA (line 252–253).

The discussion of Fig. 3 (line 208–218) needs revision. For Figures 3d, 3e, and 3f, the authors discuss the strong anti-correlated relationships, but why are these separated by case 1, 2, and 3? This is the same location and the measurements are all within a few week span, so the differences in slope and intercept are curious. Discussion of the physical meaning should be provided (e.g., what explanation is there for the greater sensitivity of H^+ to pH in case 1?). It would probably be more instructive to combine these into one plot. For Figures 3g, 3h, and 3i, what explanation do the authors have for a linear relationship between H+ and TWSII on a semi-log plot? For a given TWSII concentration, the H+ level appears to vary by several orders of magnitude, which seems to agree with Guo et al. (2015), Hennigan et al. (2015) and Murphy et al. (2017).

Response: Thanks for the suggestion. We have combined the figures 3d, 3e, and 3f into one plot (Fig. S4) and the figures 3g, 3h, and 3i were replaced by Table S2. In addition, we added the underlying reasons for the variations of H^+ for a given TWSII concentration (line 259–262): "Particle hydronium ion aqueous concentration depends on both the presence of ions and the amount of particle AWC (Guo et al., 2015). Moreover, H^+_{air} was closely associated with the NH_3 mixing ratios, and higher NH_3 always corresponded to lower H^+_{air} (Liu et al., 2017)".

The results in Figure S2 need much more discussion. This is not just limited to the HCl and HNO3 results, though more explanation should be provided. Typically, the model predictions of pH are validated by the predictions of NH3/NH4+, HCl/Cl-, and HNO3/NO3- partitioning in lieu of direct pH measurements. In addition to the problems with HCl and HNO3 at all sites, it looks like there are systematic differences in NHx partitioning between the model and measurements at the U-ZZ and R-PY sites. Why is that and what does this mean for the associated pH predictions at these sites?

Response: Thanks for the comments. We have enhanced this discussion (line 199–209): "Correlations between the predicted and measured HNO_3 and HCl are weak. Similar problems were found in the northeast U.S. and Beijing. These discrepancies were potentially due to measurement uncertainties brought about by low gas concentrations, the interference of coarse-mode particles, non-volatile cation measurement artifacts, uncertainties in the thermodynamic constants, and kinetic limitations to mass transfer (Ding et al., 2019, Haskins et al., 2018; Pye et al., 2019; Liu et al., 2017). Pye et al. (2019) suggested that ISORROPIA-II yields a mean activity coefficient of (H^+, Cl^-) that may result in the higher predicted HCl concentration. HNO_3 can be partition to both fine and coarse modes, thereby affecting predicted fine-mode nitrate concentrations (Nah et al., 2018). The best semi-volatile species for evaluation of pH modeling depend on the fraction of the gas phase. In this work, most of HNO_3 and HCl concentrated in the particle phase, and thus they are not suited to test the model (Guo et al., 2016)".

In addition, we have added the discussion about the differences in NH_x partitioning between the model and measurements at the U-ZZ and R-PY sites (line 185–197): "The differences in the slopes of NH_4^+ (Fig. S2b) and NH_3 (Fig. S2e) between U-ZZ and R-PY sites were probably attributed to the unbalanced charge of input WSIIs (see Text S1 for more details of calculation) with average equivalent ratios (Fig. S3) of 0.99 ± 0.13 (U-ZZ) and 1.20 ± 0.12 (R-PY). However, Song et al. (2018) argued that ion balance was not a key factor for pH calculation in the forward mode, because the forward mode calculations account for additional constraints imposed by the partitioning of semi-volatile species. To verify this, we adjusted the measured NH_4^+ concentration, which was most sensitive to pH modeling (see Section 3.3), to fit the ion balance, and reran the pH calculation. As shown in Fig. S4, re-predicted NH_4^+ and NH_3 concentrations have better performance ($r = 0.99$, $0.94 < \text{slopes} < 1.06$) with input concentrations at two sites than before. However, re-calculated pH values change slightly, and these deviations are included in the range of pH uncertainty discussed in Section 2.4. Therefore, the little differences in NH_x partitioning between the model and measurement among the five sites were acceptable for pH calculation." Moreover, the reason why the charge of ion was unbalance has been discussed in Text S1: "In addition to the measurement uncertainties, equivalent ratios lower than 1 might be attributed to the loss of cations from the volatilization of ammonium and unmeasured hydrogen ions (Meng et al., 2016). Equivalent ratios higher than 1 were most likely caused by water-soluble organic anions, CO_3^{2-} and HCO_3^- contents that were not detected in chemical analysis (Tian et al., 2018)".

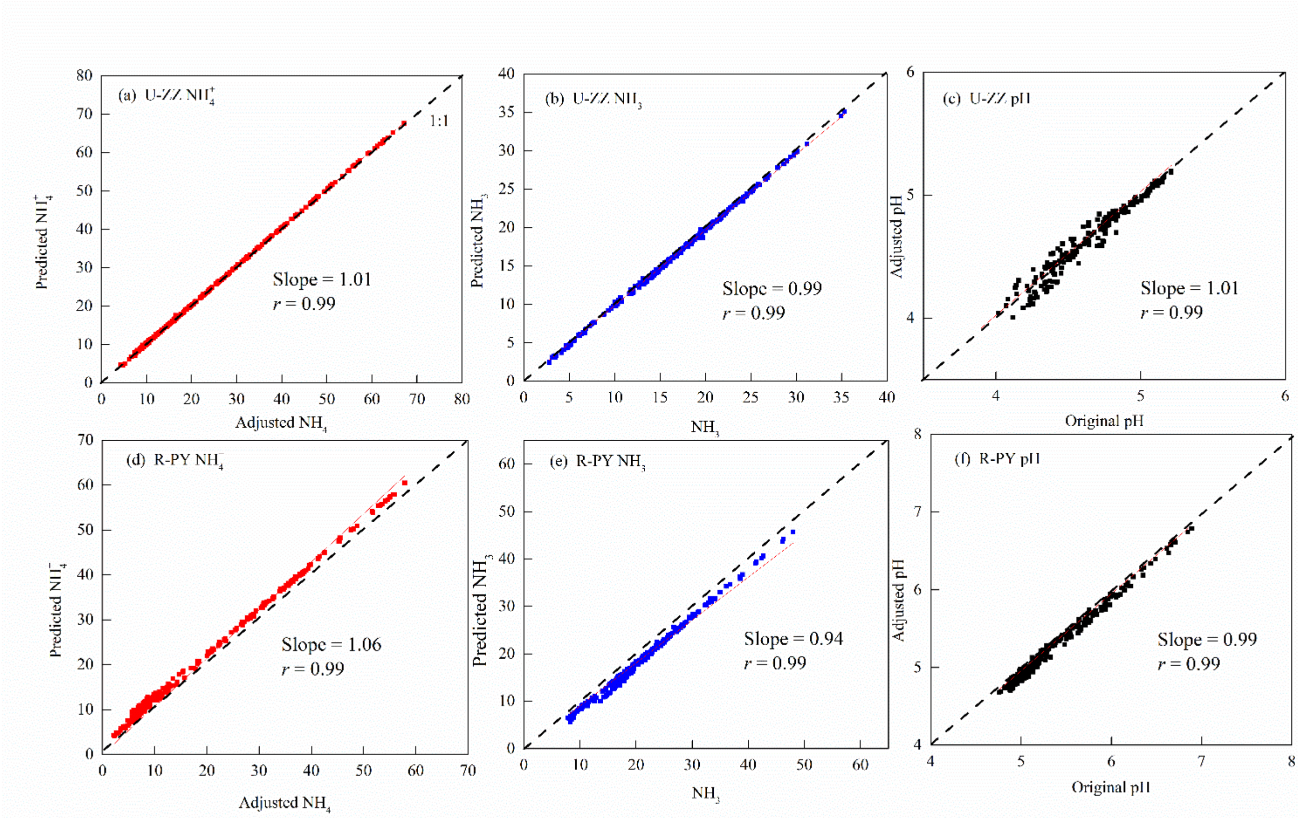

Fig. S4 Comparison between the predicted and input NH_4^+ (a, d) and NH_3 (b, c) concentrations, the original and adjusted pH (c, f) of U-ZZ and R-PY sites after adjusting the measured NH_4^+ concentrations to fit the ion balance.

Technical Corrections:

A map of the five sites should definitely be included – either in the main manuscript or supplemental.

Response: A map has been supplied in the supplemental materials (Fig. S1).

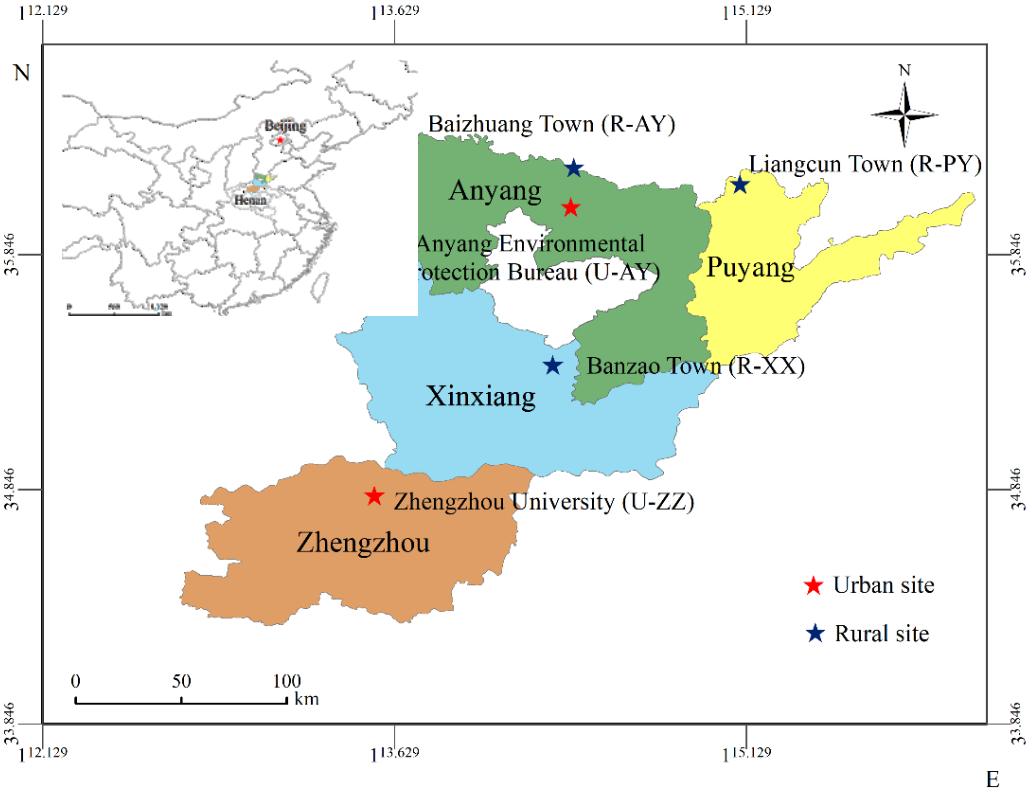

Fig. S1 Locations of the five monitoring stations in Henan Province, China (i.e., urban sites at Zhengzhou (U-ZZ) and Anyang (U-AY), rural sites at Anyang (R-AY), Xinxiang (R-XX), and Puyang (R-PY)). © 2019 National Geomatics Center of China. All rights reserved.

Line 152: ‘distraction’ is not the right term here.

Response: The “distraction” has been modified to “interference”. (L 201)

Fig. S5 needs improvement: the scale is not evident from the figures, nor is the relative locations and proximity of the five different sites.

Response: A new figure has been supplied to present the trajectory frequencies for each site during three cases with detail discussions in Text S2.

(a) Case 1

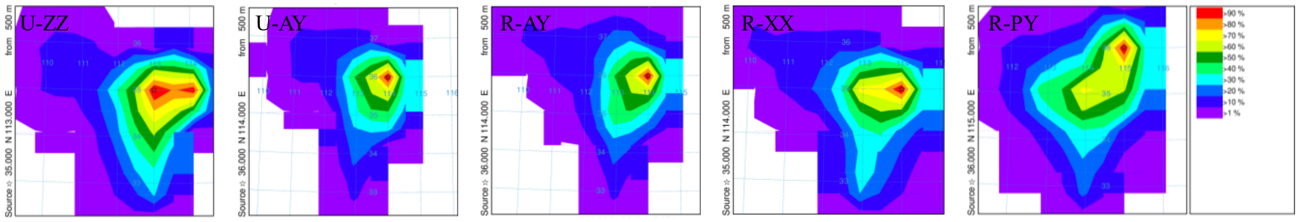

(b) Case 2

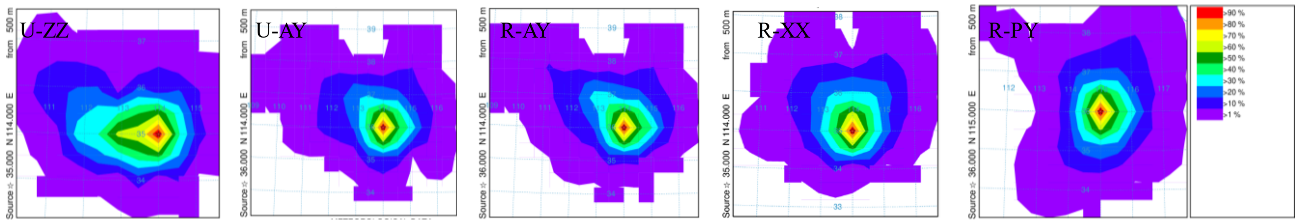

(c) Case 3

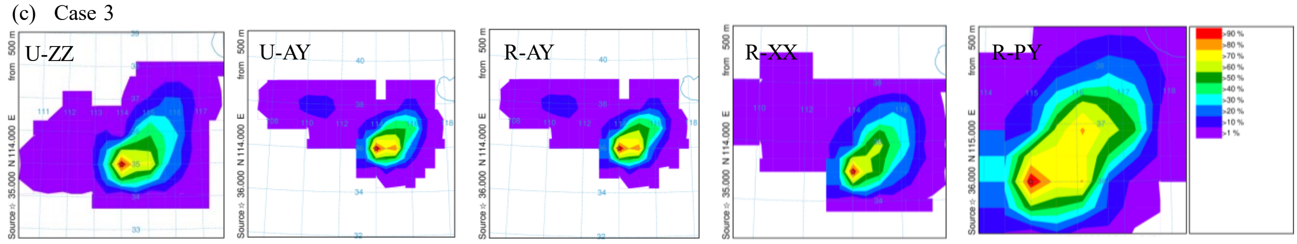

Fig. S5 Trajectory frequencies of typical periods at the five sites during Cases 1(a), 2(b), and 3(c). The color scale bar represents the percentage of trajectories passing through each grid to total trajectories.

Line 238–239: I don't see where sensitivity of pH to crustal species was analyzed?

Response: We have added the discussions on crustal species (line 297–303, 323–325): "TNa, TCl, and crustal ions (i.e., K^+, Ca^{2+}, and Mg^{2+}) have less influence on the predicted pH values, because these species were at low concentrations, together accounting for lower than 10 % of TWSIIs. However, since the low volatility of these cations allows them to preferentially neutralize sulfates over NH_3, the role of crustal dust and sea spray in particle pH cannot be ignored when the mass fraction of these ions are high in typical pollution events (e.g., sandstorm) or areas (e.g., coastland) (Allen et al., 2015; Guo et al., 2018; Vasilakos et al., 2018)", and "The crustal cations and sea spray have limited effects on pH, but a 10-fold increase in these species still can increase predicted pH values by about 0.1 units".

Line 262–263: yes, but these are presumably correlated?

Response: This sentence has been modified to "Excess-NHx concentrations may drive the pH values of rural sites higher than those of urban sites". (Line 371–372)

Line 270–271: this comment is misguided - see Weber et al (2016) for more context and explanation.

Response: This comment has been removed.

Line 286: suggest removing ‘obviously’.

Response: Done.

Lines 291-292: what is the physical meaning of these equations?

Response: These equations have been deleted and discussions on these equations have been cut down.

Line 298-299: this sentence is confusing – I suggest re-writing.

Response: This sentence has been removed.

Line 306: I’m not sure the evidence supports this statement. What about meteorology? Also, differences in local vs. regional emissions would need to be accounted for.

Response: This sentence has been modified to (line 374–378): “From the above discussion, the differences of pH among three cases indicate that the underlying influence of regional transport on local particle pH cannot be neglected by differing the chemical components of $PM_{2.5}$ and meteorological conditions. In particular, the median pH values (Table S2) of Case 1, during when the air masses transported from the south of sampling regions, increased by 0.2–0.9 units than those during Cases 2 and 3”.

Line 333: consider changing ‘promote’ to ‘perturb’?

Response: Done.

Role of ammonia on fine-particle pH in agricultural regions of China: Comparison between urban and rural sites

Shenbo Wang [a], Lingling Wang [b], Yuqing Li [c], Chen Wang [a], Weisi Wang [b], Shasha Yin [a, *], Ruiqin Zhang [a, *]

[a] *Research Institute of Environmental Science, College of Chemistry, Zhengzhou University, Zhengzhou, 450001, China*

[b] *Department of Environmental Protection of Henan Province, Zhengzhou, 450001, China*

[c] *Department of Environment Science and Engineering, Tsinghua University, Beijing 100084, China*

* Corresponding authors：Shasha Yin and Ruiqin Zhang

E-mail addresses: shashayin@zzu.edu.cn；rqzhang@zzu.edu.cn

Abstract: Particle acidity is a fundamental property that affects atmospheric particulate chemistry. Synchronous online monitoring was performed in two urban sites (e.g., Zhengzhou (U-ZZ) and Anyang (U-AY)) and three rural sites (e.g., Anyang (R-AY), Xinxiang (R-XX), and Puyang (R-PY)) in Henan Province during a haze episode to investigate the pH value and its driving factors in the agricultural regions of China. The pH values of particles calculated by ISORROPIA-II model at rural sites were slightly higher than those at urban sites, with the median (min–max) values of 5.2 (4.8–6.9, R-PY), 5.1 (4.7–6.5, R-AY), 4.9 (4.1–6.8, R-XX), 4.8 (3.9–5.9, U-AY), and 4.5 (3.8–5.2, U-ZZ). Sensitivity tests show that TNH_x (total ammonium (gas + aerosol)), followed by total sulfate, were the important factors that influenced the predicted pH. Generally, particle pH increased with the cation increasing and the decrease in the anion, temperature, and relative humidity. Similar pH values (~3.0) at the required NH_x concentrations for the five sites indicated that the presence of excess NH_x was likely important for the less acidic of $PM_{2.5}$ during the severe haze episodes in this region. Moreover, the concentrations of excess NH_x may drive the higher pH values at rural sites, because of the higher excess NH_x concentrations at rural sites than those at urban sites. The underlying influence of regional transport on local particle pH cannot be neglected by differing the chemical components of $PM_{2.5}$ and meteorological conditions. Air masses transported from rural and agricultural regions may enhance the particle pH value in urban aerosols given the high pH of particles and high ammonia levels. These results suggest that ammonia is urgently needed to be involved in the regional strategy for the improvement of air quality in China.

Keywords: ISORROPIA-II model, Particle acidity, Ammonia, Sensitivity test, Regional transport.

1 Introduction

High concentrations of acids and bases contained in the aqueous phase define the acidity of aerosols (Spurny, 1990). Particle acidity or pH value is an important parameter for atmospheric particulate chemistry, such as the gas-particle portioning of semi-volatile and volatile species (e.g., $NH_{3(g)}/NH_{4(aq)}^{+}$, $HCl_{(g)}/Cl_{(aq)}^{-}$, and $HNO_{3(g)}/NO_{3(aq)}^{-}$), the formation of secondary inorganic and organic aerosols, and the dissolution of metallic elements (Bougiatioti et al., 2016; Meskhidze et al., 2003; Seinfeld and Pandis, 2006; Shi et al., 2019; Shi et al., 2010; Surratt et al., 2010; Wang et al., 2018b). Particle acidity can affect the ecosystem through its influence on wet/dry deposition, atmospheric visibility, and radiative balance (Boucher and Anderson, 1995; Larssen et al., 2006; Pye et al., 2019; Watson, 2002). In addition, high particle acidity has an adverse impact on public health, especially for the cardiopulmonary and respiration system of humans (Dockery et al., 1996; Ostro et al., 1991).

Direct measurements on particle pH are challenging because of the small size and nonideality of chemical species in solvated aerosols. Therefore, thermodynamic models, such as E-AIM (http://www.aim.env.uea.ac.uk/aim/aim.php) and ISORROPIA-II (http://isorropia.eas.gatech.edu) (Clegg et al., 1998; Nenes et al., 1998), which rely on the measurements of particulate and gaseous species, are widely used in estimating particle pH. Generally, the global distribution of fine particulate matter ($PM_{2.5}$, aerodynamic diameter ≤ 2.5 μm) pH is bimodal with a population of particles having a mean pH of 1–3 and another population having an average pH closer to 4–5 (Pye et al., 2019). Table 1 shows that $PM_{2.5}$ in mainland China were moderately acidic with pH values that ranged from 3.4–5.7 (Ding et al., 2019; Guo et al., 2017; Liu et al., 2017; Shi et al., 2017, 2019; Song et al., 2018; Wang et al., 2019a), which were 3–5 units higher than those reported in other regions, such as Hong Kong, Singapore, USA, and Greece (Behera et al., 2013; Bougiatioti et al., 2016; Guo et al., 2016; Guo et al., 2014; Pathak et al., 2004).

High atmospheric ammonia (TNH_x, gas NH_3 plus particle NH_4^+) is a dominant factor that drives the high $PM_{2.5}$ pH in megacities of China because it suppresses the production of particle hydronium (Cheng et al., 2016; Wang et al., 2016). Liu et al. (2017) argued that excess NH_3 and elevated aerosol water content (AWC) were responsible for the high pH in Beijing. Nevertheless, Guo et al. (2017) and Song et al. (2018) demonstrated that high levels of ammonia did not increase the $PM_{2.5}$ pH into a fully neutralized condition in Beijing and Xi'an, China. Weber et al. (2016) calculated that only large increases in NH_3 together with sulfate reductions can lead to an increase in pH. Correspondingly, higher pH by about 1 unit than urban aerosols was observed in locations of intensive agriculture with high NH_3 concentrations in the southeastern US (Nah et al., 2018). The primary sources for ammonia include agricultural emissions, such as livestock waste, N-fertilizer application, and biomass burning, as well as traffic and industrial emissions (Huang et al., 2012; Shen et al., 2011; Wang et al., 2018a). Field studies have reported that elevated NH_3 and NH_4^+ concentrations were recorded at rural sites in the North China Plain (Meng et al., 2011; Meng et al., 2017; Shen et al., 2011; Wen et al., 2015). Therefore, studying in an agriculturally developed region is needed to obtain insight into the role of ammonia in particle pH. Unfortunately, previous studies mainly concentrated on calculating the particle pH in the megacity of China, and few studies focused on the agricultural regions of China. In addition to ammonia, particle pH can also be influenced by other chemical compositions and meteorological conditions, such as sulfate, AWC, temperature (T), and relative humidity (RH). Sulfate is often the main acid component of aerosols, and largely determines the acidity of $PM_{2.5}$ (Weber et al., 2016). Sensitivity tests in Beijing suggested that sulfate, TNH_x, and T were the common driving factors, and Ca^{2+} and RH were the unique factors in special seasons (Ding et al., 2019). The pH sensitivity based on the 10-year record in Canada showed that chemical compositions had various effects on particle pH under different meteorological conditions; moreover, careful examination for any particular region is needed (Tao and Murphy, 2019).

Henan Province is situated in Central China; it has a dense rural population and is a top-ranking province in China in terms of agricultural production and chemical fertilizer consumption (NBS, 2016). NH_3 emission inventory for Henan Province reported that approximately 1031.6 Gg NH_3 was released in Henan in 2015, thereby contributing to approximately 10 % of China's total emissions (approximately 10 Tg) (Huang et al., 2012; Wang et al., 2018a). Livestock waste and N-fertilizer application were major sources for ammonia emissions, which may increase TNH_x concentrations at rural sites than in urban sites. Furthermore, Henan Province is a severely $PM_{2.5}$-polluted region in China. In January 2018, a large-scale and long-lasting haze episode that caused $PM_{2.5}$ concentration to reach 400 μg/m^3 occurred in this region (Wang et al., 2019c). An experiment was performed in two urban and three rural sites in Henan Province to investigate the particle acidity and its driving factor. ISORROPIA-II model was utilized to estimate $PM_{2.5}$ pH using a high-time-resolution dataset. The novelty of the work addressed in the present study is that this study is the first on $PM_{2.5}$ acidity by comparing urban and rural sites in the agricultural regions of China. The specific objectives of the study were presented as follows: (1) Estimation and comparison of the $PM_{2.5}$ pH at the five monitoring sites, (2) identification of the factors that determine the pH, and (3) discussion of the role of ammonia on pH. Our results are helpful to understand the factors that determine particle acidity better.

2 Experiment and methods

2.1 Site descriptions

Field sampling was synchronously conducted from January 12 to 24, 2018 at five sites (i.e., two urban sites located in the center of Zhengzhou (U-ZZ) and Anyang (U-AY), and three sites located in the rural areas of Anyang (R-AY), Xinxiang (R-XX), and Puyang (R-PY)). Locations of the five sites (Fig. S1) with brief descriptions are listed in Table 2. U-ZZ site is surrounded by busy roads, and two freeways are located 3 km to the south and 7 km to the east. Moreover, this site is near a coal-fired power plant; a gas-fired power plant; and several small-scale industries, such as pharmaceutical companies, electronic factories, and equipment manufacturing. U-AY site is surrounded by busy roads, and Anyang steelwork is located 8 km to the west. R-AY site is surrounded by farmland and is 1 km west of the Jing-Gang-Ao freeway and 1 km north of a belt freeway. R-XX and R-PY sites are surrounded by farmland without other prominent anthropogenic emission sources.

2.2 Instrumentations

The hourly mass concentrations of water-soluble inorganic ions (WSIIs) in $PM_{2.5}$, such as NH_4^+, SO_4^{2-}, NO_3^-, Cl^-, Na^+, Mg^{2+}, Ca^{2+}, and K^+ and their gaseous precursors (i.e., NH_3, HNO_3, and HCl) were measured using an ambient ion monitor (URG-9000D, Thermal Fisher Scientific, USA) in U-ZZ site and the monitor for aerosols and gases (MARGA, Metrohm, Switzerland) in other sites. Both instruments have been successfully deployed in several other field experiments (Li et al., 2017; Shi et al., 2017; Wang 2019b), and detailed information is available elsewhere (Markovic et al., 2012; Rumsey et al., 2014). As a brief summary, ambient air is drawn into the systems at a flow rate of 16.7 L/min. Subsequently, particles and gases are collected by two aerosol sample collectors through a wet parallel plate or wet rotating denuder. Aqueous solution samples are quantified by using two ion chromatography analyzers. Detection limits for all species during the sampling periods were less than 0.1 μg/m^3. Measurement uncertainties were assumed to 10 % for URG-9000D here by reference to 10 % of Markovic et al. (2012) and 12 % in Hu et al. (2014). For the MARGA instrument, Song et al. (2018) took 20 % as overall relative uncertainties for major species, and Rumsey et al. (2014) reported that the analytical biases were lower than 10 % for SO_4^{2-}, NO_3^-, and HNO_3, but higher than 15 % for NH_3 and NH_4^+. Therefore, overall uncertainties were estimated to be 20 % for NH_3 and NH_4^+ and 10 % for other species. The combined uncertainties for TNH_x were calculated to be 14 % and 23 % for U-ZZ and other sites, respectively, and 14 % uncertainties of TNO_3 ($NO_{3(aq)}^-$ + $HNO_{3(g)}$) and TCl ($Cl_{(aq)}^-$ + $HCl_{(g)}$) for all sites. Because of the complex interference during sampling periods at the five sites, such as the slope from the internal calibration, the solution volume, temperature, pressure, and airflow rate, the actual uncertainties might be different from the estimated value. Hourly elemental carbon (EC) and organic carbon (OC) concentrations in $PM_{2.5}$ were simultaneously obtained by the semi-continuous carbon analyzers (Model 4, Sunset Laboratory Inc, USA) in the same place, except for the U-ZZ site, of which data were provided by the Department of Environmental Protection of Henan Province. Detailed information on this instrument can be found in Panteliadis et al. (2014). Briefly, $PM_{2.5}$ collected by the device was oxidized to carbon dioxide and analyzed by a nondispersive infrared detector. The relative measurement uncertainty for this instrument was estimated to be 20 % (Liu et al., 2013; Healy et al., 2013). Meteorological parameters, including T, RH, wind direction, and wind speed, were recorded by smart weather sensor (LUFFT-WS500, Sutron Corporation, Germany), with the accuracies of ± 0.2 °C, ± 2 %, < 3 °, and 0.1 m/s, respectively.

2.3 pH prediction

Particle pH was estimated using the ISORROPIA-II thermodynamic model. Input data, including RH, T, concentrations of K^+, Ca^{2+}, Mg^{2+}, TNH_x, total sulfate (TH_2SO_4, replaced by observed SO_4^{2-}), total sodium (TNa, replaced by observed Na^+), TCl, and TNO_3, were used to calculate the particle hydronium ion concentration per volume of air (H^+_{air}) and particle water associated with inorganics (AWC_{inorg}) by computing the equilibrium composition for the Na^+-K^+-Ca^{2+}-Mg^{2+}-NH_4^+-SO_4^{2-}-NO_3^--Cl^--H_2O aerosol system. Considering that forward mode is less sensitive to measurement error than the reverse mode and high RH levels were recorded in sampling periods, ISORROPIA-II was run in the forward model for the aerosol system in the metastable condition (Ding et al, 2019; Guo et al., 2015; Hennigan et al., 2015). Moreover, we excluded data with RH < 30 %, a condition where predicted to observed partitioning of nitrate between the gas and particle phase are in weak correlation, and thus uncertainties in the pH prediction are expected to be high (Ding et al., 2019; Guo et al., 2016). Aerosol pH was calculated according to the formula (Bougiatioti et al., 2016):

$$\mathrm{pH} = -\log_{10} H^+_{aq} = -\log_{10} \frac{1000 H^+_{air}}{AWC_{inorg} + AWC_{org}}, \tag{1}$$

where the modeled concentrations for AWC_{inorg} and H^+_{air} are μg/m^3, and AWC_{org} is the particle water associated with the organics predicted using the method:

$$AWC_{org} = \frac{m_s}{\rho_s} \frac{k_{org}}{\left(\frac{1}{\mathrm{RH}} - 1\right)}, \tag{2}$$

where m_s is the mass concentrations of organic matter (OC × 1.6), ρ_s is the organic density (1.35 g/cm^3), and k_{org} is the organic hygroscopicity parameter (0.06) (Liu et al., 2017).

2.4 pH uncertainty

Two extreme scenarios were evaluated to estimate the pH uncertainty based on the measurement uncertainties of input data (Murphy et al., 2017). Sensitivity tests of pH to input data (see Section 3.3) suggest that simulated pH increase with the cation concentrations (i.e., TNH_x, TNa, K^+, Ca^{2+}, and Mg^{2+}) increasing as well as the anion concentrations (i.e., TH_2SO_4, TNO_3, and TCl), T and RH decreasing. Moreover, the pH value has a positive correlation with OC concentrations via Eqs. (1 and 2). Therefore, cation and OC concentrations were adjusted up to within their maximum positive uncertainties, and anions, RH and T were adjusted down within their maximum negative uncertainties, which represented the pH_{max} case; for pH_{min} case, cations and OC concentrations were adjusted down, and anions, RH and T were adjusted up. Figure 1 suggests that pH_{max} cases lead to 6 % (slope − 1) errors for all sites, and pH_{min} cases can result in approximately 10 % deviations. Thus, pH uncertainties were set to be −9–6 %, −13–6 %, −12–6 %, −11–6 %, and −10–5 % for U-ZZ, U-AY, R-AY, R-XX, and R-PY sites, respectively.

2.5 Model validation

The reliability of pH estimation using the ISORROPIA-II thermodynamic model depends on several assumptions, such as the equilibrated gas and particle phases (Pye et al., 2019). Thus, the predicted and observed semi-volatile species (e.g., $NH_{3(g)}/NH_{4(aq)}{}^+$, $HCl_{(g)}/Cl_{(aq)}{}^-$, and $HNO_{3(g)}/NO_{3(aq)}{}^-$) are compared in Fig. S2. Observed and predicted NH_4^+, Cl^-, and NO_3^- exhibit significant correlations, have correlation coefficients (*r*) above 0.95 and slopes near 1 at the five sites. In addition, NH_3 concentrations are in good agreement ($r > 0.95$) with slopes between 0.89 (U-ZZ) and 1.13 (R-PY). These results suggest the excellent performance of ISORROPIA-II for modeling these species. The differences in the slopes of NH_4^+ (Fig. S2b) and NH_3 (Fig. S2e) between U-ZZ and R-PY sites were probably attributed to the unbalanced charge of input WSIIs (see Text S1 for more details of calculation) with average equivalent ratios (Fig. S3) of 0.99 ± 0.13 (U-ZZ) and 1.20 ± 0.12 (R-PY). However, Song et al. (2018) argued that ion balance was not a key factor for pH calculation in the forward mode, because the forward mode calculations account for additional constraints imposed by the partitioning of semi-volatile species. To verify this, we adjusted the measured NH_4^+ concentration, which was most sensitive to pH modeling (see Section 3.3), to fit the ion balance, and reran the pH calculation. As shown in Fig. S4, re-predicted NH_4^+ and NH_3 concentrations have better performance ($r = 0.99$, $0.94 < \text{slopes} < 1.06$) with input concentrations at two sites than before. However, re-calculated pH values change slightly, and these deviations are included in the range of pH uncertainty discussed in Section 2.4. Therefore, the little differences in NH_x partitioning between the model and measurement among the five sites were acceptable for pH calculation.

Correlations between the predicted and measured HNO_3 and HCl are weak. Similar problems were found in the northeast U.S. and Beijing. These discrepancies were potentially due to measurement uncertainties brought about by low gas concentrations, the interference of coarse-mode particles, non-volatile cation measurement artifacts, uncertainties in the thermodynamic constants, and kinetic limitations to mass transfer (Ding et al., 2019, Haskins et al., 2018; Pye et al., 2019; Liu et al., 2017). Pye et al. (2019) suggested that ISORROPIA-II yields a mean activity coefficient of (H^+, Cl^-) that may result in the higher predicted HCl concentration. HNO_3 can be partition to both fine and coarse modes, thereby affecting predicted fine-mode nitrate concentrations (Nah et al., 2018). The best semi-volatile species for evaluation of pH modeling depend on the fraction of the gas phase. In this work, most of HNO_3 and HCl concentrated in the particle phase, and thus they are not suited to test the model (Guo et al., 2016).

The $PM_{2.5}$ pH was also calculated by the E-AIM (Version IV) model to evaluate the performance of ISORROPIA-II using the observed data (RH > 60 %) of the U-ZZ site as an example. Close correlation ($r = 0.89$) is found between two models with a slope of 0.95 (Fig. S5). The pH values in ISORROPIA-II are 0.46 ± 0.15 units higher than those in E-AIM. These values are comparable to the founding by Liu et al. (2017) and Song et al. (2018), which is possibly due to the differences of activity coefficient values between the ISORROPIA-II and E-AIM models (Pye et al., 2019). Overall, the predicted pH values using ISORROPIA-II are effective in this work.

3 Results and discussion

3.1 Haze episodes

During the sampling periods, five monitoring sites simultaneously experienced a long-lasting and large-scale haze episode. Time series of the concentrations of major species (i.e., NH_3, NH_4^+, SO_4^{2-}, and NO_3^-) and meteorological parameters at the U-ZZ site as an example are presented in Fig. 2, and other sites are integrated into Fig S6 with the mean values listed in Table 3. Three study cases were classified on the basis of similar meteorological conditions and WSIIs levels at the five sites. The WSIIs concentration, T, and RH gradually increased in the southern wind during Case 1 (January 12−14). Case 3 (January 21–25) was characterized by decreased WSII concentrations, T, and RH with the northeastern wind. Even though the total WSIIs (TWSIIs) concentrations were comparable, the chemical components of WSIIs were various between Cases 1 and 3 (Table 3). In particular, NO_3^-, NH_4^+, and NH_3 concentrations in Case 1 were higher than those in Case 3 at all sites. Conversely, SO_4^{2-} concentrations in Case 1 were lower than those in Case 3. Wang et al. (2018a) reported that the southern cities of Henan Province (e.g., Nanyang, Shangqiu, Zhoukou, and Zhumadian) had relatively higher ammonia emissions than the cities involved in this study. Moreover, the northeastern air masses from the Jing–Jin–Ji regions were easily enriched with sulfate (Wang et al., 2019b; Wang et al., 2018c). Evidently, back trajectory frequency analysis (see Text S2 for more details of the discussion) confirmed that sampling sites during Cases 1 and 3 (Figs. S7a and c) were predominantly influenced by the southern and northeastern air masses, respectively.

Elevated WSIIs concentrations during Case 2 (January 14–21) were under high T and RH conditions with variable wind directions. In this case, local emissions played a key role in WSIIs (Fig. S7b) with average NH_4^+, SO_4^{2-}, and NO_3^- concentrations that ranged from 31.9 ± 12.5 μg/m^3 (U-ZZ) to 47.6 ± 13.1 μg/m^3 (R-AY), 32.9 ± 12.5 μg/m^3 (R-XX) to 46.8 ± 16.9 μg/m^3 (R-AY), and 58.0 ± 18.3 μg/m^3 (U-AY) to 76.8 ± 21.1 μg/m^3 (R-AY), respectively. Note that higher concentrations of NH_4^+, NH_3, and TNH_x during Case 2 were recorded at rural sites than those at urban sites. Moreover, NH_3 levels in this work were higher than those in other studies summarized in Table S1. Agricultural emissions, including livestock waste, N-fertilizer application, and humans, were the top three ammonia contributors in Henan Province (Wang et al., 2018a), which may result in elevated ammonia concentrations at rural sites.

3.2 pH of $PM_{2.5}$ at the urban and rural sites

Figure 3 exhibits the predicted $PM_{2.5}$ pH values, H^+_{air}, and AWC at the five sites, pH uncertainties based on the pH_{max} and pH_{min} calculations are presented in Fig. S8. $PM_{2.5}$ have consistent moderate acidity during this haze episode, with median (min–max) pH values of 4.5 (3.8–5.2), 4.8 (3.9–5.8), 4.9 (4.1–6.2), 5.1 (4.7–6.3), and 5.2 (4.8–6.5,) at U-ZZ, U-AY, R-XX, R-AY, and R-PY, respectively. As summarized in Table 1, $PM_{2.5}$ pH values were close to the results of other cities in China (e.g., Beijing, Xi'an, and Tianjin), but higher than other countries (e.g., Singapore, USA, and Greece). Compared to the rural sites in the USA, pH values were roughly 3 units higher at the R-AY, R-XX, and R-PY sites. Moreover, statistical values of pH (Table S2) during three cases show higher pH values at rural sites than those at urban sites, especially for the U-ZZ and R-PY sites during Case 1 despite their pH uncertainties (Section 2.4).

The pH values (Table S2) of the five sites during Cases 2 and 3 were comparable but slightly lower than those during Case 1. As shown in Fig. S9, predicted pH values present better correlations with H^+_{air} concentrations rather than AWC. Particle hydronium ion aqueous concentration depends on both the presence of ions and the amount of particle AWC (Guo et al., 2015). Moreover, H^+_{air} was closely associated with the NH_3 mixing ratios, and higher NH_3 always corresponded to lower H^+_{air} (Liu et al., 2017). High correlations ($r > 0.5$) between H^+_{air} and TWSIIs (Table S3) imply that local pH was significantly affected by the TWSIIs levels, and probably resulting in the high acidity during Case 2. H^+_{air} was also correlated with individual chemical species (e.g., TNH_x, TH_2SO_4, TNO_3, and TCl). Therefore, the diversity of pH in Cases 1 and 3 may be partly owing to the different proportions of particle- and gas-phase constituents that will be discussed in detail below. In addition, high correlations between RH and H^+_{air} (Table S3) suggest the major role of meteorological conditions in particle pH. Given the Case 2 was less affected by regional transport, the diurnal patterns of median pH values of the five sites (Fig. 4) indicate that pH values during nighttime were 0.3 (R-PY)–0.5 (U-ZZ) units higher than those during the daytime. Similar results were also found in other cities (e.g., Beijing, Tianjin, southern Canada, and the USA) (Battaglia et al., 2017; Ding et al., 2019; Guo et al., 2015; Murphy et al., 2017; Shi et al., 2019), resulting from the diurnal trends of T and RH (Fig. 4f). After sunrise, high

T facilitated the dissociation of particle-phase ammonium (e.g., NH_4NO_3) and led to a rapid loss of AWC (Guo et al., 2015; Saraswati et al., 2019).

3.3 Sensitivity tests of pH

To explore the dominant factors that determine the local particle pH level and resulting in the high pH at rural sites, sensitivity tests of pH to chemical species (i.e., TNH_x, TH_2SO_4, TNO_3, TCl, TNa, K^+, Ca^{2+}, and Mg^{2+}) and meteorological parameters (i.e., T and RH) were performed. Firstly, the real-time measured values of a variable (e.g., TNH_x) and average values of other parameters (i.e., TH_2SO_4, TNO_3, TCl, TNa, K^+, Ca^{2+}, Mg^{2+}, T and RH) during Case 2 were input into ISORROPIA-II to investigate the sensitivity of local pH to this variable (i.e., TNH_x) (Ding et al., 2019), and results are listed in Table 4 and Fig. S10. In addition, a given range for a variable for all sites with corresponding average values of other parameters was simulated to compare its effects on pH among five sites (Figs. 5 and S11). The chosen variation range for each variable was close to the observed minimum and maximum values (Table S4), which aims to better reflect the actual observation conditions. The degree of sensitivity was represented as the relative standard deviation (%RSD) of the re-calculated pH values. RSD calculates the absolute value of the coefficient of variation, which helps us to determine how small or large is the standard deviation when compared to the mean of the re-calculated pH data set. Therefore, when the re-calculated pH data set has a higher RSD value, this variable can change the pH easier and is more important for local pH.

As shown in Table 4, the most important factor that influenced particle pH during Case 2 was TNH_x, followed by TH_2SO_4 at the five sites, and the U-ZZ site was also affected by TNO_3. The acidity of $PM_{2.5}$ is governed by the phase partitioning of semi-volatile gases such as NH_3, HNO_3, and HCl

(Pye et al., 2019). $(NH_4)_2SO_4$, NH_4HSO_4, and NH_4NO_3, which are mainly formed through neutralization reactions between NH_3 with SO_4^{2-} and HNO_3 orderly according to the regime of local ammonia, are the most abundant components of $PM_{2.5}$ in winter haze in this region (Wang et al., 2019c; Pathak et al., 2008). Therefore, particle pH was driven by TNH_x, TH_2SO_4, and TNO_3. TNa, TCl, and crustal ions (i.e., K^+, Ca^{2+}, and Mg^{2+}) have less influence on the predicted pH values, because these species were at low concentrations, together accounting for lower than 10 % of TWSIIs. However, since the low volatility of these cations allows them to preferentially neutralize sulfates over NH_3, the role of crustal dust and sea spray in particle pH cannot be ignored when the mass fraction of these ions are high in typical pollution events (e.g., sandstorm) or areas (e.g., coastland) (Allen et al., 2015; Guo et al., 2018; Vasilakos et al., 2018). In addition to chemical species, T was more sensitive to local pH than RH at the five sites, which is similar to the finding in Beijing and Canada (Ding et al., 2019; Tao and Murphy, 2019). This result can be explained by the remarkable influence of T on the solubility and dissociation constants of the partitioning of $NH_{3(g)}/NH_{4(aq)}^+$ (Hennigan et al., 2015).

Figures 5 and S11 compare the sensitive degrees of pH to input data among different sites. Except for TNH_x, the sensitivities of pH to TH_2SO_4, TNO_3, and other ions at urban sites were more significant than those at rural sites, particularly at U-ZZ sites of 7.2 % and 14.8 % of RSD to TH_2SO_4 and TNO_3, respectively. To gain insight into the differences of pH sensitivity among the five sites, sensitivity tests of pH to TH_2SO_4, TNO_3, and TNH_x were calculated using the fixed TNO_3 (67.5 μg/m^3) and TH_2SO_4 (36.5 μg/m^3) concentrations under the average meteorological conditions of five sites (i.e., T = 2.5 °C and RH = 60 %). These chosen values were close to the average values of the five sites during Case 2 (i.e., 36.4 ± 15.4 μg/m^3 for SO_4^{2-}, 67.5 ± 23.5 μg/m^3 for TNO_3, 2.5 ± 1.5 °C for T, and 59.3 ±14.0 %

for RH), and other chemical species were set to be zero. As shown in Fig. 6, sensitivities of pH to TH_2SO_4 and TNO_3 increase with the decrease in TNH_x concentration, particularly when the TNH_x concentrations are lower than 60 μg/m^3 and 40 μg/m^3, respectively. Therefore, the pH changes tended to become more sensitive to TH_2SO_4 and TNO_3 at the U-ZZ site (Fig. 5e, f) with the lowest TNH_x concentrations (46.8 ± 14.7 μg/m^3). All these results may be explained by the presence of excess ammonia that will be discussed below.

Sensitivity tests suggest (Fig. 5, S10, and S11) that particle pH gradually grows with increased cation and decreased anion concentrations. Specifically, the TNH_x concentration that increased from 25 μg/m^3 to 90 μg/m^3 can promote particle pH by 3.5 (U-ZZ)–4.5 (R-AY) units. The crustal cations and sea spray have limited effects on pH, but a 10-fold increase in these species still can increase predicted pH values by about 0.1 units. TH_2SO_4, and TNO_3 that increased from 10 μg/m^3 to 80 μg/m^3, and 1 μg/m^3 to 125 μg/m^3 can reduce the pH values by 1.5 (R-PY)–4.0 (U-ZZ), and 0.2 (R-AY)–1.4 (U-ZZ) units, respectively. In addition, a 20 °C (–5 °C to 15 °C) and 65 % (30 % to 95 %) increase drops the pH by approximately 1.3 and 2.7 units at the five sites, respectively. Corresponding to the observed data during Case 2 (Table 3), lower TNH_x concentrations and higher T values were probably responsible for the higher acidity at urban sites than those at rural sites. Moreover, Figure 6 shows that particle pH increase with decreasing TH_2SO_4 (Fig. 6a) or increasing TNO_3 (Fig. 6b), particularly when the TNH_x is at high concentration. These results indicate that predicted pH will be enhanced by increasing the TNO_3/TH_2SO_4 ratio, which is consistent with the observation in Beijing (Xie et al., 2019). All these may be due to the elevated ammonia partitioning with nitrate fraction increase, and nitrate-rich particles would absorb more water compared to the sulfate-rich particles (Xie et al., 2019).

Based on the above, higher TNH_x (Table 3) and TNO_3/TH_2SO_4 ratios (2.9 ± 0.6 and 1.7 ± 0.6 for Cases 1 and 3 respectively) during Case 1 may lead to the higher pH values than those during Case 3, even though the TWSIIs levels were comparable. In the long run, the decreasing sulfate concentration in $PM_{2.5}$ accompanied with increasing nitrate concentration has been recorded during haze episodes in China, because strong actions were taken to reduce the coal consumption in recent years (Tian et al., 2017; Wang et al., 2017). Considering the ammonia in the atmosphere of North China might still be increasing (Liu et al., 2018), future acidity of $PM_{2.5}$ during winter haze episodes is expected to become increasingly less acidic in this area. A more careful analysis is needed to test this inference, however, because fine-mode particle remains a relatively constant pH of 0–2 despite a 70 % reduction in sulfates in the USA (Vasilakos et al., 2018; Weber et al., 2016).

3.4 Role of ammonia on pH

It has been suggested that unusually high levels of NH_3 can increase pH, on average, a 5-fold to 10-fold increase in the NH_3 levels leads to a one-unit change in pH (Nah et al., 2018; Weber et al., 2016; Guo et al., 2017). To examine the effects of major indicators of ammonia (i.e., TNH_x, Required-NH_x, and Excess-NH_x, see Text S3 for more details of calculation) on aerosol acidity, particle pH was calculated by using a wide range of TNH_x (25–130 $\mu g/m^3$) and average values of other parameters during Case 2 (Table 3) of each site. Simultaneously, the concentrations of TNH_x, Required-NH_x, Excess-NH_x, and corresponding pH values are illustrated in Fig. 7. An "*S*-curve" growth trend of pH to increasing TNH_x appears with the inflection point around the Required-NH_x concentration. In the case when the input TNH_x concentration is lower than the Required-NH_x, the growth rate of pH increase with TNH_x increasing, otherwise, the pH growth flattens out, which is similar to the findings of Weber et al. (2016) and Bougiatioti et al. (2016). In the process of increasing NH_3 concentration, NH_3 reacted with SO_4^{2-} and HNO_3 orderly, during when large amounts of H^+ were consumed and pH values rapidly increased. Theoretically, the Required-NH_x plus nonvolatile cations can neutralize all anions regardless of the phase partitioning and bisulfate formation, and thus changes in TNH_x around the Required-NH_x concentrations have a significant impact on particle pH. Subsequently, dissolving Excess-NH_x into the particles became difficult, and pH values increased slowly (Ding et al., 2019; Seinfeld and Pandis, 2016). Therefore, the underlying reason why TNH_x concentrations lower than 60 μg/m^3 and 40 μg/m^3 elevated the pH sensitivities (Fig. 6) to TH_2SO_4 and TNO_3 is that the Excess-NH_x will be exhausted under the case of TH_2SO_4 and TNO_3 that ranged from 10 μg/m^3 to 100 μg/m^3, respectively. On the other hand, the pH values of the five sites at the Required-NH_x concentrations are near 3.0, which is in coincidence with the pH value of Beijing in the no-excess-NH_x cases (Liu et al., 2017). Therefore, the presence of Excess-NH_x in the aerosol was likely important for the less acidic of $PM_{2.5}$ and can enhance the pH values by 1.5 (U-ZZ)–2 (R-PY) units. Considering that the Excess-NH_x concentrations at rural sites (e.g., 30.1 ± 6.2 μg/m^3 at R-PY) were higher than those at urban sites (e.g., 14.8 ± 4.1 μg/m^3 at U-ZZ), and thus Excess-NH_x concentrations may drive the pH values of rural sites higher than those of urban sites.

3.5 Implications of regional transport

From the above discussion, the differences of pH among three cases indicate that the underlying influence of regional transport on local particle pH cannot be neglected by differing the chemical components of $PM_{2.5}$ and meteorological conditions. In particular, the median pH values (Table S2) of Case 1, during when the air masses transported from the south of sampling regions, increased by 0.2–

0.9 units than those during Cases 2 and 3. Aqueous formations of sulfate are strongly dependent on particle pH. Chen et al. (2016) reported that the aqueous-phase sulfate production rates from NO_2 and O_3 oxidation of SO_2 had a positive correlation with particle pH during the Beijing haze events. When pH exceeded approximately 4.5 (higher than this value at rural sites in this work), NO_2-oxidation dominated the sulfate formation, and its reaction rate increased by one order of magnitude with the rise of pH by one unit. Thus, air masses transported from rural and agricultural regions may promote the sulfate formation in urban aerosols. In addition to sulfate, higher aerosol pH favors partitioning of TNO_3 toward aerosol NO_3 rather than gaseous HNO_3 and thus elevating the particle mass concentration (Nenes et al., 2019; Weber et al., 2016). Sampling regions in this study are located in the transport route for Beijing (MEP, 2017), thereby frequently affecting its local particle pH. The lifetimes of NH_3 (1–5 days or less) and NH_4^+ (1–15 days) in the atmosphere are sufficient for transporting to Beijing during a haze episode (Aneja, 2000; Lefer et al., 1999; Warneck, 1988). Ding et al. (2019) have also observed that $PM_{2.5}$ pH from the southwest direction was generally higher than that from the northern direction in Beijing. Therefore, the particle pH in Beijing may be enhanced when southern air masses from this region accompany elevated-pH particles and high ammonia levels.

4 Conclusions

An experiment was performed using a series of high-time-resolution instruments in two urban (i.e., U-ZZ and U-AY) and three rural sites (i.e., R-AY, R-XX, and R-PY) in Henan Province during a large-scale and long-lasting haze episode. The ISORROPIA-II model was used to investigate the pH value and its driving factors. $PM_{2.5}$ exhibited moderate acidity with median pH values of 4.5 (3.8–5.2), 4.8 (3.9–5.8), 4.9 (4.1–6.2), 5.1 (4.7–6.3), and 5.2 (4.8–6.5,) at U-ZZ, U-AY, R-XX, R-AY, and R-PY, respectively. The pH values at rural sites were slightly higher than those at urban sites.

The predicted pH values of $PM_{2.5}$ were significantly affected by the WSIIs levels, different proportions of particle- and gas-phase constituents, and meteorological parameters. Sensitivity tests show that TNH_x, followed by TH_2SO_4, were the important factors that influenced the predicted pH at the five sites. In addition, T was more sensitive to local pH than RH. Generally, particle pH rose with the increase in cation and the decrease in the anion, T, and RH. Further study suggests that predicted pH will be enhanced by increasing the TNO_3/TH_2SO_4 ratio. Therefore, elevated TNH_x concentrations and lower T were probably responsible for the higher pH values at rural sites than those at urban sites, and higher TNH_x and TNO_3/TH_2SO_4 ratios during Case 1 may lead to the higher pH values than those during Case 3.

An “*S*-curve” growth trend of pH to increasing TNH_x was found with the inflection point around the Required-NH_x concentration. Moreover, the pH values of the five sites at the Required-NH_x concentrations are near 3.0, and the presence of Excess-NH_x in the aerosol can enhance the pH values by 1.5 (U-ZZ)–2 (R-PY) units, and thus Excess-NH_x was likely important for the less acidic of $PM_{2.5}$ during the severe haze episodes in this region. Considering that the Excess-NH_x concentrations at rural sites were higher than those at urban sites, Excess-NH_x concentrations may drive the pH values of rural sites higher than those of urban sites.

The underlying influence of regional transport on local particle pH cannot be neglected by differing the chemical components of $PM_{2.5}$ and meteorological conditions. Air masses transported from rural and agricultural regions with elevated pH particles and high ammonia levels may promote the secondary particle formation in urban aerosols. Therefore, ammonia should be involved in the regional strategy for improving the air quality in China.

Data availability. All data in this work are available by contacting the corresponding author Shasha Yin (shashayin@zzu.edu.cn)

Author contributions. Shasha Yin and Ruiqin Zhang designed and led this study. Shasha Yin was responsible for all observations and data collection. Lingling Wang, Yuqing Li, Chen Wang, and Weisi Wang interpreted the data and discussed the results. Shenbo Wang wrote the paper.

Competing interests. The authors declare that they have no conflict of interest.

Acknowledgment

This work was supported by the National Key R&D Program of China (No. 2017YFC0212403) and the National Natural Science Foundation of China (No. 41907187). We thank Qi Hao and Liuming Yang for their contributions to the field observations.

References

Allen, H. M., Draper, D. C., Ayres, B. R., Ault, A., Bondy, A., Takahama, S., Modini, R. L., Baumann, K., Edgerton, E., Knote, C., Laskin, A., Wang, B., and Fry, J. L.: Influence of crustal dust and sea spray supermicron particle concentrations and acidity on inorganic NO_3^- aerosol during the 2013 Southern Oxidant and Aerosol Study. Atmos. Chem. Phy., 15, 10669−10685, 2015.

Aneja, V. P., Chauhan, J. P., Walker, J. T.: Characterization of atmospheric ammonia emissions from swine waste storage and treatment lagoons. J. Geophy. Res.-Atmos., 105, 11535−11545, 2000.

Battaglia, M. A., Douglas, S., and Hennigan, C. J.: Effect of the urban heat island on aerosol pH, Environ. Sci. Technol., 51, 13095−13103, 2017.

Behera, S. N., Betha, R., Liu, P., Balasubramanian, R.: A study of diurnal variations of $PM_{2.5}$ acidity and related chemical species using a new thermodynamic equilibrium model. Sci. Total Environ., 452, 286−295, 2013.

Boucher, O., Anderson, T. L.: General circulation model assessment of the sensitivity of direct climate forcing by anthropogenic sulfate aerosols to aerosol size and chemistry. J. Geophy. Res.-Atmos., 100, 26117−26134, 1995.

Bougiatioti, A., Nikolaou, P., Stavroulas, I., Kouvarakis, G., Weber, R., Nenes, A., Kanakidou, M., Mihalopoulos, N.: Particle water and pH in the eastern Mediterranean: source variability and implications for nutrient availability. Atmos. Chem. Phy., 16, 4579−4591, 2016.

Bureau of Statistics of Henan (NBH), 2018. Henan Statistical Yearbook. China Statistics Press, Beijing. Accessed date: Dec. 2019.

Cheng, Y., Zheng, G., Wei, C., Mu, Q., Zheng, B., Wang, Z., Gao, M., Zhang, Q., He, K., Carmichael, G.: Reactive nitrogen chemistry in aerosol water as a source of sulfate during haze events in China. Sci. Adv., 2, e1601530−e1601530, 2016.

Clegg, S. L., Brimblecombe, P., Wexler, A. S.: The thermodynamic model of the system $H^+-NH_4^+-SO_4^{2-}-NO_3^--H_2O$ at tropospheric temperatures. J. Phy. Chem. A, 102, 2137−2154, 1998.

Ding, J., Zhao, P., Su, J., Dong, Q., Du, X., Zhang, Y.: Aerosol pH and its driving factors in Beijing. Atmos. Chem. Phy., 19, 7939−7954, 2019.

Dockery, D. W., Cunningham, J., Damokosh, A. L., Neas, L. M., Spengler, J. D., Koutrakis, P., Ware, J. H., Raizenne, M., Speizer, F. E.: Health effects of acid aerosols on North American children: respiratory symptoms. Environ. Health Persp., 104, 500−505, 1996.

Guo, H., Sullivan, A. P., Campuzanojost, P., Schroder, J. C., Lopezhilfiker, F. D., Dibb, J. E., Jimenez, J. L., Thornton, J. A., Brown, S. S., Nenes, A.: Fine particle pH and the partitioning of nitric acid during winter in the northeastern United States. J. Geophy. Res.-Atmos., 121, 10−355, 2016.

Guo, H., Weber, R. J., Nenes, A.: High levels of ammonia do not raise fine particle pH sufficiently to yield nitrogen oxide-dominated sulfate production. Sci. Rep., 7, 12109, 2017.

Guo, H., Xu, L., Bougiatioti, A., Cerully, K. M., Capps, S. L., Hite, J. R., Carlton, A. G., Lee, S., Bergin, M. H., Ng, N. L.: Fine-particle water and pH in the southeastern United States. Atmos. Chem. Phy., 15, 5211−5228, 2015.

Guo, H., Nenes, A., and Weber, R. J.: The underappreciated role of nonvolatile cations on aerosol ammonium-sulfate molar ratios, Atmos. Chem. Phys., 18, 17307–17323, 2018.

Haskins, J. D., Jaegle, L., Shah, V., Lee, B. H., Lopez-Hilfiker, F. D., Campuzano-Jost, P., Schroder, J. C., Day, D. A., Guo, H. Y., Sullivan, A. P., Weber, R., Dibb, J., Campos, T., Jimenez, J. L., Brown, S. S., and Thornton, J. A.: Wintertime gas-particle partitioning and speciation of inorganic chlorine in the lower troposphere over the northeast United States and coastal ocean, J. Geophys. Res.-Atmos., 123, 12897−12916, 2018

Healy, R. M., Sciare, J., Poulain, L., Crippa, M., Wiedensohler, A., Prévôt, A. S. H., Baltensperger, U., Sarda-Estève, R., McGuire, M. L., Jeong, C.-H., McGillicuddy, E., O'Connor, I. P., Sodeau, J. R., Evans, G. J., and Wenger, J. C.: Quantitative determination of carbonaceous particle mixing state in Paris using single-particle mass spectrometer and aerosol mass spectrometer measurements, Atmos. Chem. Phys., 13, 9479–9496, 2013.

Hennigan, C. J., Izumi, J., Sullivan, A. P., Weber, R. J., and Nenes, A.: A critical evaluation of proxy methods used to estimate the acidity of atmospheric particles, Atmos. Chem. Phys., 15, 2775–2790, 2015.

Hu, G., Zhang, Y., Sun, J., Zhang, L., Shen, X., Lin, W., Yang, Y.: Variability, formation and acidity of water-soluble ions in $PM_{2.5}$ in Beijing based on the semi-continuous observations. Atmos. Res., 145, 1−11, 2014.

Huang, X., Song, Y., Li, M., Li, J., Huo, Q., Cai, X., Zhu, T., Hu, M., Zhang, H.: A high-resolution ammonia emission inventory in China. Global Biogeochem. Cy., 26, GB1030, 2012.

Larssen, T., Lydersen, E., Tang, D., He, Y., Gao, J., Liu, H., Duan, L., Seip, H .M., Vogt, R. D., Mulder, J.: Acid rain in China. Environ. Sci. Technol., 40, 418−425, 2006.

Lefer, B. L., Talbot, R. W., Munger, J. W.: Nitric acid and ammonia at a rural northeastern US site. J. Geophy. Res.-Atmos., 104, 1645−1661, 1999.

Li, Y. J., Sun, Y., Zhang, Q., Li, X., Li, M., Zhou, Z., Chan, C. K.: Real-time chemical characterization of atmospheric particulate matter in China: A review. Atmos. Environ., 158, 270−304, 2006.

Liu, J., Bergin, M., Guo, H., King, L., Kotra, N., Edgerton, E., Weber, R. J.: Size-resolved measurements of brown carbon in water and methanol extracts and estimates of their contribution to ambient fine-particle light absorption. Atmos. Chem. Phy., 13, 12389−12404, 2013.

Liu, M., Song, Y., Zhou, T., Xu, Z., Yan, C., Zheng, M., Wu, Z., Hu, M., Wu, Y., Zhu, T.: Fine particle pH during severe haze episodes in northern China. Geophys. Res. Lett., 44, 5213−5221, 2017.

Liu, W., Lin, S., and Hu, G.: Characterizing remarkable changes of severe haze events and chemical compositions in multi-size airborne particles (PM_1, $PM_{2.5}$ and PM_{10}) from January 2013 to 2016−2017 winter in Beijing, China, Atmos. Environ., 189, 133−144, 2018.

Markovic, M. Z., Vandenboer, T. C., Murphy, J. G.: Characterization and optimization of an online system for the simultaneous measurement of atmospheric water-soluble constituents in the gas and particle phases. J Environ. Monitor., 14, 1872−1884, 2012.

Meng, Z., Lin, W., Jiang, X., Yan, P., Wang, Y., Zhang, Y. M., Jia, X. F., Yu, X. L.: Characteristics of atmospheric ammonia over Beijing, China. Atmos. Chem. Phy., 11, 6139−6151, 2011.

Meng, Z., Xu, X., Lin, W., Ge, B., Xie, Y., Song, B., Jia, S., Zhang, R., Peng, W., Wang, Y.: Role of ambient ammonia in particulate ammonium formation at a rural site in the North China Plain. Atmos. Chem. Phy., 18, 167−184, 2017.

MEP: 2017 air pollution prevention and management plan for the Beijing-Tianjin-Hebei region and its surrounding areas, http://dqhj.mee.gov.cn/dtxx/201703/t20170323_408663.shtml (last access: 18 August 2019), 2017.

Meskhidze, N., Chameides, W. L., Nenes, A., Chen, G.: Iron mobilization in mineral dust: Can anthropogenic SO_2 emissions affect ocean productivity? Geophys. Res. Lett., 30, 2003.

Murphy, J. G., Gregoire, P. K., Tevlin, A. G., Wentworth, G. R., Ellis, R. A., Markovic, M. Z., VandenBoer, T. C.: Observational constraints on particle acidity using measurements and modelling of particles and gases, Faraday Discuss., 200, 379−395, 2017.

Nah, T., Guo, H., Sullivan, A. P., Chen, Y., Tanner, D. J., Nenes, A., Russell, A., Ng, L. N., Huey, L. G., Weber, R. J.: Characterization of aerosol composition, aerosol acidity, and organic acid partitioning at an agriculturally intensive rural southeastern US site. Atmos. Chem. Phy. 18, 11471−11491. 2018.

National Bureau of Statistics (NBS), 2016. China Statistical Yearbook. China Statistics Press, Beijing. Accessed date: Sept. 2019.

Nenes, A., Pandis, S. N., Pilinis, C.: ISORROPIA: A new thermodynamic equilibrium model for multiphase multicomponent inorganic aerosols. Aquat. Geochem., 4, 123−152, 1998.

Nenes, A., Pandis, S. N., Weber, R. J., and Russell, A.: Aerosol pH and liquid water content determine when particulate matter is sensitive to ammonia and nitrate availability, Atmos. Chem. Phys. Discuss., in review, 2019.

Ostro, B., Lipsett, M., Wiener, M.B., Selner, J.C.: Asthmatic responses to airborne acid aerosols. Am. J. Public Health, 81, 694−702, 1991.

Panteliadis, P., Hafkenscheid, T., Cary, B., Diapouli, E., Fischer, A., Favez, O., Quincey, P., Viana, M., Hitzenberger, R., Vecchi, R.: ECOC comparison exercise with identical thermal protocols after temperature offset correction: instrument diagnostics by in-depth evaluation of operational parameters. Atmos. Meas. Tech., 8, 779−792, 2014.

Pathak, R. K., Louie, P. K., Chan, C. K.: Characteristics of aerosol acidity in Hong Kong. Atmos. Environ., 38, 2965−2974, 2004.

Pathak, R.K., Wu, W.S., Wang, T.: Summertime $PM_{2.5}$ ionic species in four major cities of China: nitrate formation in an ammonia-deficient atmosphere. Atmos. Chem. Phys. 9, 1711–1722, 2008.

Pye, H. O. T., Nenes, A., Alexander, B., Ault, A. P., Barth, M. C., Clegg, S. L., Collett Jr., J. L., Fahey, K. M., Hennigan, C. J., Herrmann, H., Kanakidou, M., Kelly, J. T., Ku, I.-T., McNeill, V. F., Riemer, N., Schaefer, T., Shi, G., Tilgner, A., Walker, J. T., Wang, T., Weber, R., Xing, J., Zaveri, R. A., and Zuend, A.: The acidity of atmospheric particles and clouds, Atmos. Chem. Phys. Discuss., in review, 2019.

Rumsey, I. C., Cowen, K. A., Walker, J. T., Kelly, T. J., Hanft, E. A., Mishoe, K., Rogers, C., Proost, R., Beachley, G. M., Lear, G.: An assessment of the performance of the Monitor for AeRosols and GAses in ambient air (MARGA): a semi-continuous method for soluble compounds. Atmos. Chem. Phy., 14, 5639−5658, 2014.

Saraswati, Sharma, S. K., Saxena, M., Mandal, T. K.: Characteristics of gaseous and particulate ammonia and their role in the formation of secondary inorganic particulate matter at Delhi, India. Atmos. Res., 218, 34−49, 2019.

Seinfeld, J. H. and Pandis, S. N.: Atmospheric Chemistry and Physics: From Air Pollution to Climate Change, 2nd Edition, John Wiley and Sons, Inc., Hoboken, New Jersey, USA, 2006.

Seinfeld, J. H. and Pandis, S. N.: Atmospheric Chemistry and Physics: From Air Pollution to Climate Change (3rd edition), John Wiley and Sons, Inc., Hoboken, New Jersey, USA, 2016.

Shen, J., Liu, X., Ying, Z., Fangmeier, A., Goulding, K., Zhang, F.: Atmospheric ammonia and particulate ammonium from agricultural sources in the North China Plain. Atmos. Environ., 45, 5033−5041, 2011.

Shi, G., Xu, J., Peng, X., Xiao, Z., Chen, K., Tian, Y., Guan, X., Feng, Y., Yu, H., Nenes, A.: pH of aerosols in a polluted atmosphere: source contributions to highly acidic aerosol. Environ. Sci. Technol., 51, 4289−4296, 2017.

Shi, X., Nenes, A., Xiao, Z., Song, S., Yu, H., Shi, G., Zhao, Q., Chen, K., Feng, Y., Russell, A. G.:

High-resolution data sets unravel the effects of sources and meteorological conditions on nitrate and its gas-particle partitioning. Environ. Sci. Technol., 53, 3048−3057, 2019.

Shi, Z., Bonneville, S., Krom, M. D., Carslaw, K. S., Jickells, T. D., Baker, A. R., Benning, L. G.: Iron dissolution kinetics of mineral dust at low pH during simulated atmospheric processing. Atmos. Chem. Phy., 11, 995−1007, 2010.

Song, S., Gao, M., Xu, W., Shao, J., Shi, G., Wang, S., Wang, Y., Sun, Y., Mcelroy, M. B.: Fine particle pH for Beijing winter haze as inferred from different thermodynamic equilibrium models. Atmos. Chem. Phy., 18, 7423−7438, 2018.

Spurny, K. R.: Atmospheric acidic aerosols (review). J Aerosol Sci., 21, 1990.

Surratt, J. D., Chan, A. W. H., Eddingsaas, N. C., Chan, M. N., Loza, C. L., Kwan, A. J., Hersey, S., Flagan, R. C., Wennberg, P. O., Seinfeld, J. H.: Reactive intermediates revealed in secondary organic aerosol formation from isoprene. P. Natl. Acad. Sci. USA., 107, 6640−6645, 2010.

Tao, Y. and Murphy, J. G.: The sensitivity of $PM_{2.5}$ acidity to meteorological parameters and chemical composition changes: 10-year records from six Canadian monitoring sites. Atmos. Chem. Phy.. 19, 9309−9320, 2019.

Tian, M., Wang, H., Chen, Y., Zhang, L., Shi, G., Liu, Y., Yu, J., Zhai, C., Wang, J., Yang, F.: Highly time-resolved characterization of water-soluble inorganic ions in $PM_{2.5}$ in a humid and acidic mega city in Sichuan Basin, China. Sci. Total Environ., 580, 224−234, 2017.

Vasilakos, P., Russell, A., Weber, R., and Nenes, A.: Understanding nitrate formation in a world with less sulfate, Atmos. Chem. Phys., 18, 12765–12775, 2018.

Wang, C., Yin, S., Bai, L., Zhang, X., Gu, X., Zhang, H., Lu, Q., Zhang, R.: High-resolution ammonia emission inventories with comprehensive analysis and evaluation in Henan, China, 2006–2016. Atmos. Environ., 193, 11−23, 2018a.

Wang, G., Zhang, F., Peng, J., Duan, L., Ji, Y., Marreroortiz, W., Wang, J., Li, J., Wu, C., Cao, C.: Particle acidity and sulfate production during severe haze events in China cannot be reliably inferred by assuming a mixture of inorganic salts. Atmos. Chem. Phy., 18, 1−23, 2018b.

Wang, G., Zhang, R., Gomez, M. E., Yang, L., Levy, Z. M., Hu, M., Lin, Y., Peng, J., Guo, S., Meng, J.: Persistent sulfate formation from London Fog to Chinese haze. P. Natl. Acad. Sci. USA., 113, 13630−13635, 2016.

Wang, H., Ding, J., Xu, J., Wen, J., Han, J., Wang, K., Shi, G., Feng, Y., Ivey, C., Wang, Y.: Aerosols in an arid environment: The role of aerosol water content, particulate acidity, precursors, and relative humidity on secondary inorganic aerosols. Sci. Total Environ., 646, 564−572, 2019a.

Wang, J., Zhao, B., Wang, S., Yang, F., Xing, J., Morawska, L., Ding, A., Kulmala, M., Kerminen, V., Kujansuu, J.: Particulate matter pollution over China and the effects of control policies. Sci. Total Environ., 584, 426−447, 2017.

Wang, S., He, B., Yuan, M., Su, F., Yin, S., Yan, Q., Jiang, N., Zhang, R., Tang, X.: Characterization of individual particles and meteorological conditions during the cold season in Zhengzhou using a single particle aerosol mass spectrometer. Atmos. Res., 219, 13−23, 2019b.

Wang, S., Yan, Q., Yu, F., Wang, Q., Yang, L., Zhang, R., Yin, S., Wang, S., Yan, Q., Yu, F.: Distribution and source of chemical elements in size-resolved particles in Zhengzhou, China: Effects of regional transport. Aerosol Air Qual. Res., 18, 371−385, 2018c.

Wang, S., Yin, S., Zhang, R., Yang, L., Zhao, Q., Zhang, L., Yan, Q., Jiang, N., Tang, X.: Insight into the formation of secondary inorganic aerosol based on high-time-resolution data during haze episodes and snowfall periods in Zhengzhou, China. Sci. Total Environ., 660, 47−56, 2019c.

Warneck, P.: Chemistry of the Natural Atmosphere, Academic Press, San Diego, CA, 1988.

Watson, J. G.: Visibility: science and regulation. J Air Waste Manage., 52, 973−999, 2002.

Weber, R. J., Guo, H., Russell, A. G., and Nenes, A.: High aerosol acidity despite declining atmospheric sulfate concentrations over the past 15 years, Nat. Geosci., 9, 282−285, 2016.

Wen, L., Chen, J., Yang, L., Wang, X., Xu, C., Sui, X., Yao, L., Zhu, Y., Zhang, J., Zhu, T.: Enhanced formation of fine particulate nitrate at a rural site on the North China Plain in summer: The important roles of ammonia and ozone. Atmos. Environ., 101, 294−302, 2015.

Xie, Y., Wang, G., Wang, X., Chen, J., Chen, Y., Tang, G., Wang, L., Ge, S., Xue, G., Wang, Y., and Gao, J.: Observation of nitrate dominant $PM_{2.5}$ and particle pH elevation in urban Beijing during the winter of 2017, Atmos. Chem. Phys. Discuss., in review, 2019.

Figure lists:

Fig. 1 pH uncertainties of the five sites based on two extreme scenarios of measurement uncertainty. Cations and organic carbon concentrations (OC) were adjusted up to within their maximum positive uncertainties, anions, relative humidity (RH) and temperature (T) were adjusted down within their maximum negative uncertainties, which represented the pH_{max} case; for pH_{min} case, cations and OC concentrations were adjusted down, and anions, RH and T were adjusted up. The color scale bar represents adjusted RH.

Fig. 2 Temporal variations of T, RH, wind speed (WS), wind direction (WD), and concentrations of NH_3, NH_4^+, SO_4^{2-}, and NO_3^- during three cases at the Zhengzhou (U-ZZ) site. The shaded areas represent the measurement uncertainties.

Fig. 3 Time series and box plot of predicted $PM_{2.5}$ pH, H^+_{air}, and aerosol water content (AWC) at the five sites. In each box, the top, middle and bottom lines represent the 75th, 50th, and 25th percentile of statistical data, respectively; the upper and lower whiskers represent the maximum and minimum values, respectively.

Fig. 4 (a)–(e) Diurnal patterns of median pH values, (f) average RH, and T of the five sites in Case 2. The upper and lower ends of the line represent the maximum and minimum values of pH, respectively. The color scale bar represents AWC concentration.

Fig. 5 Comparison of the sensitivities of $PM_{2.5}$ pH to T, RH, TCl ($HCl_{(g)} + Cl_{(aq)}^-$), TNH_x ($NH_{3(g)} + NH_{4(aq)}^+$), TNO_3 ($HNO_{3(g)} + NO_{3(aq)}^-$), and TH_2SO_4 (replaced by observed SO_4^{2-}) among the five sites. A given range for a variable for all sites with corresponding average values of other parameters was used as input to the ISORROPIA-II model. The range of the x-axis is close to the observed minimum and maximum values in Case 2 (Table S4). The color scale bar represents the pH values. The relative standard deviation (RSD) and range (Range) represent the sensitivity degree of pH to this variable and range (min–max) of the re-predicted pH value in the test, respectively. The square plots on the graph represent the average values of each variable observed in Case 2 with standard deviation as an error bar.

Fig. 6 Particle pH calculated with fixed meteorological parameters (T = 275.5 K and RH = 60 %) under different combinations of TNH_x and (a) TH_2SO_4 (Fixed TNO_3 = 67.5 μg/m^3) and (b) TNO_3 (Fixed TH_2SO_4 = 36.5 μg/m^3). The color scale bar represents the pH values. The markers on the graph represent the average concentrations of TNH_x, TH_2SO_4, and TNO_3 at the five sites during Case 2 with standard deviation as error bar.

Fig. 7 Particle pH corresponds to increasing TNH_x at the five sites to examine the effects of major indicators of NH_3 (i.e., TNH_x, Required-NH_x, and Excess-NH_x) on aerosol acidity. Particle pH was calculated by using a wide range of TNH_x (25–130 μg/m^3) and average values of other parameters during Case 2 of each site. The concentrations of TNH_x, Required-NH_x, and Excess-NH_x with corresponding pH values are marked by a hollow box, hollow circle, and arrow respectively. The yellow and blue background colors correspond to the NH_x-poor and NH_x-rich, respectively.

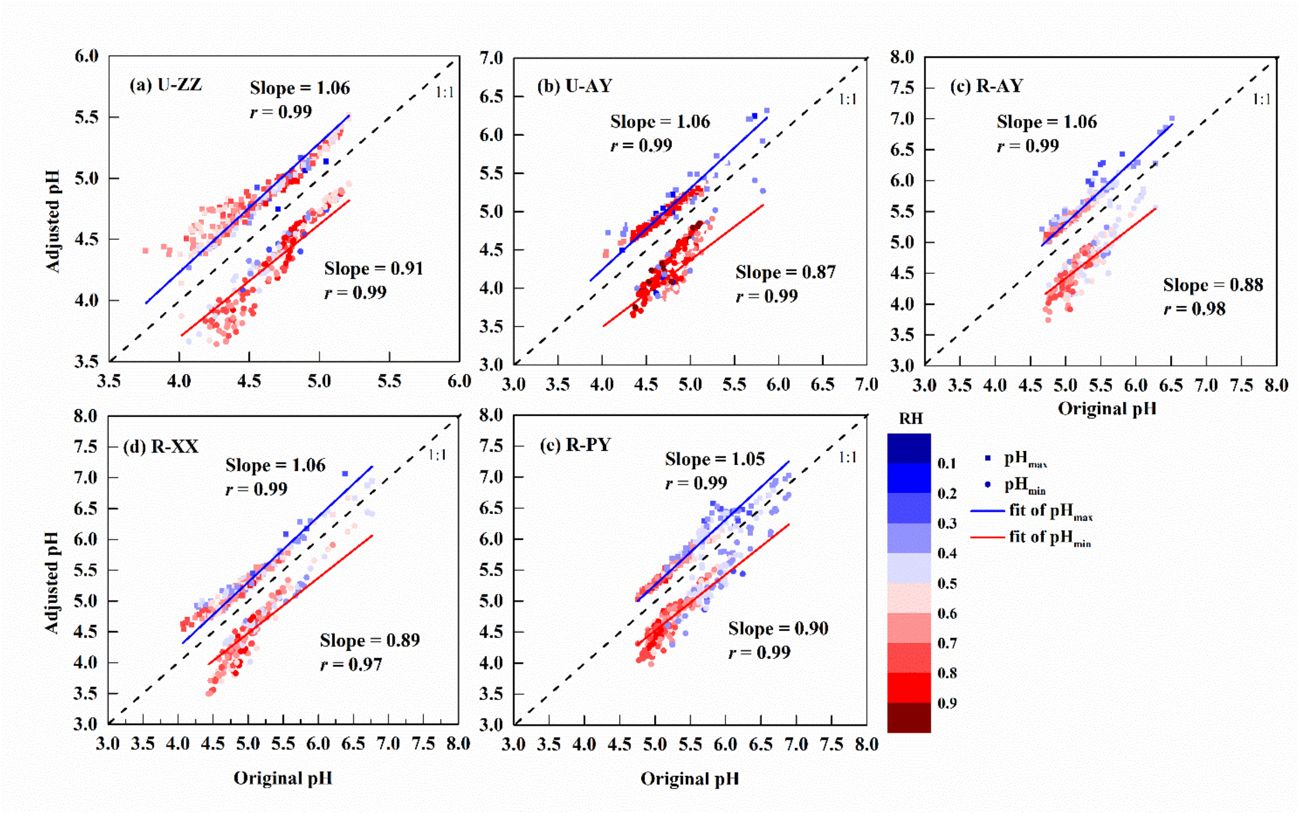

Fig. 1 pH uncertainties of the five sites based on two extreme scenarios of measurement uncertainty. Cations and organic carbon concentrations (OC) were adjusted up to within their maximum positive uncertainties, anions, relative humidity (RH) and temperature (T) were adjusted down within their maximum negative uncertainties, which represented the pH_{max} case; for pH_{min} case, cations and OC concentrations were adjusted down, and anions, RH and T were adjusted up. The color scale bar represents adjusted RH.

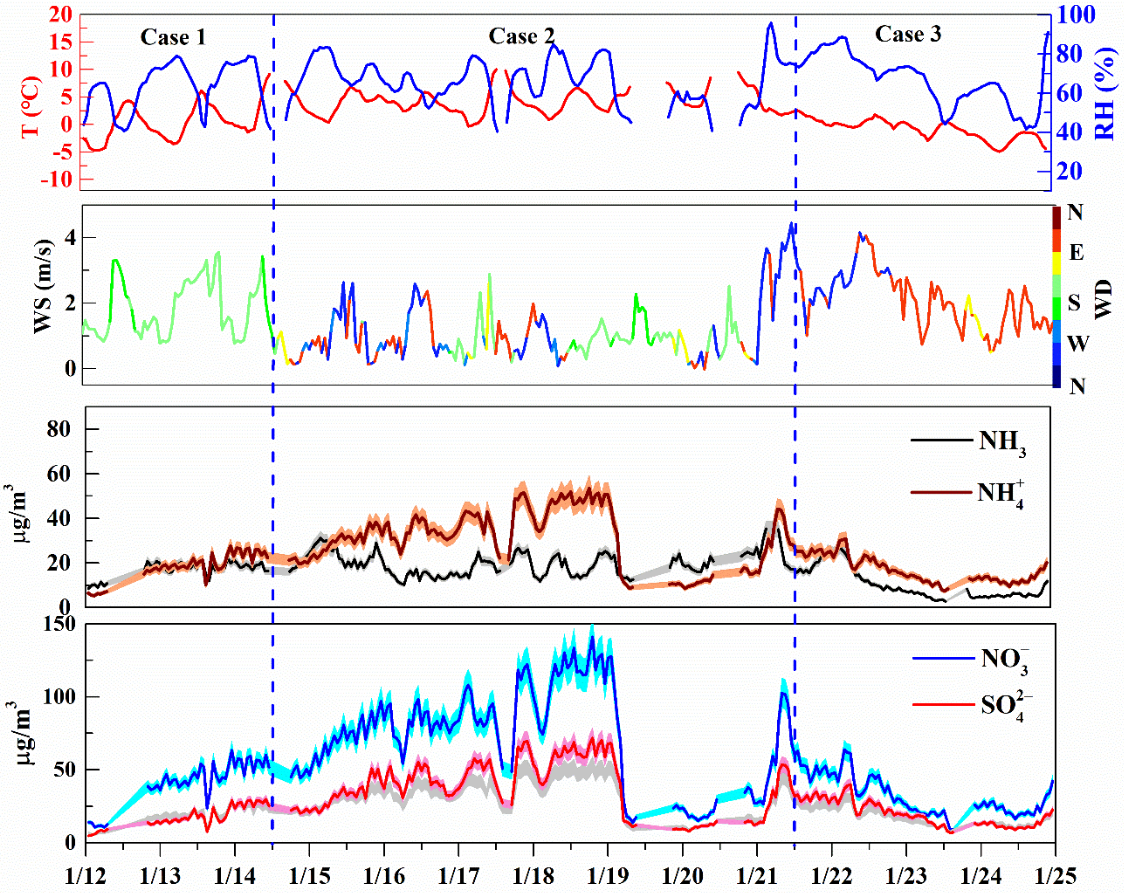

Fig. 2 Temporal variations of T, RH, wind speed (WS), wind direction (WD), and concentrations of NH_3, NH_4^+, SO_4^{2-}, and NO_3^- during three cases at the Zhengzhou (U-ZZ) site. The shaded areas represent the measurement uncertainties.

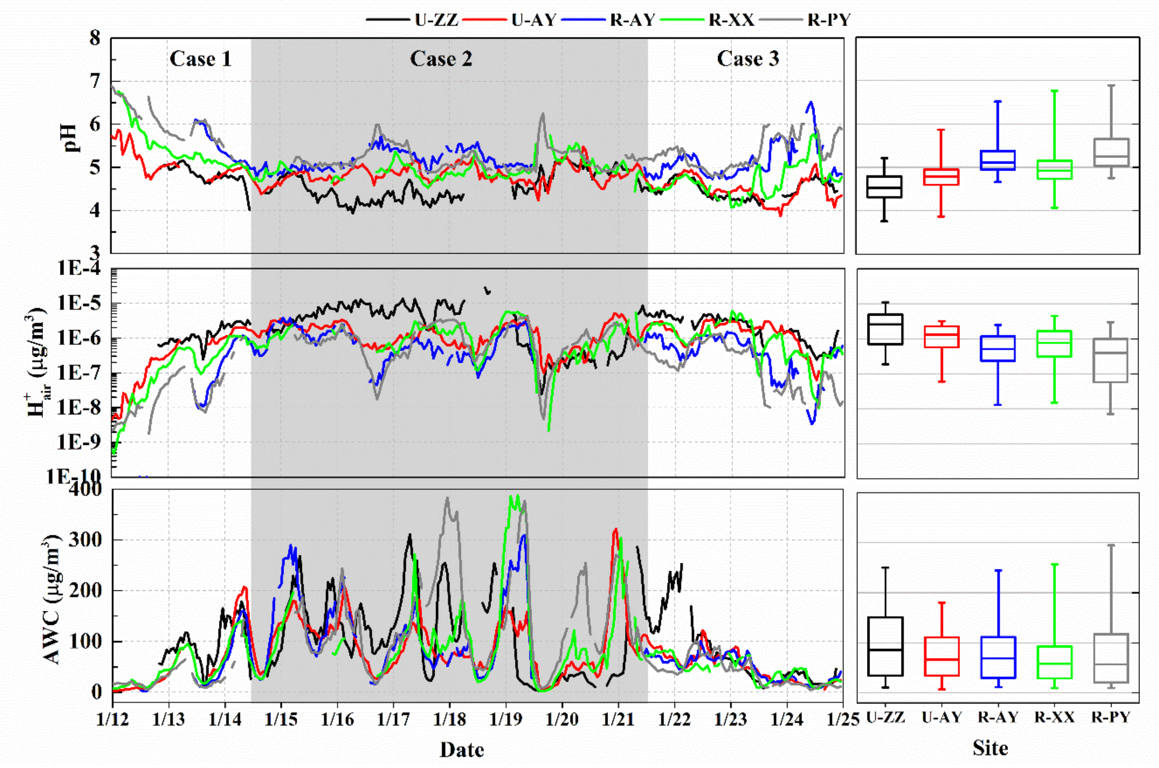

Fig. 3 Time series and box plot of predicted $PM_{2.5}$ pH, H^{+}_{air}, and aerosol water content (AWC) at the five sites. In each box, the top, middle and bottom lines represent the 75th, 50th, and 25th percentile of statistical data, respectively; the upper and lower whiskers represent the maximum and minimum values, respectively.

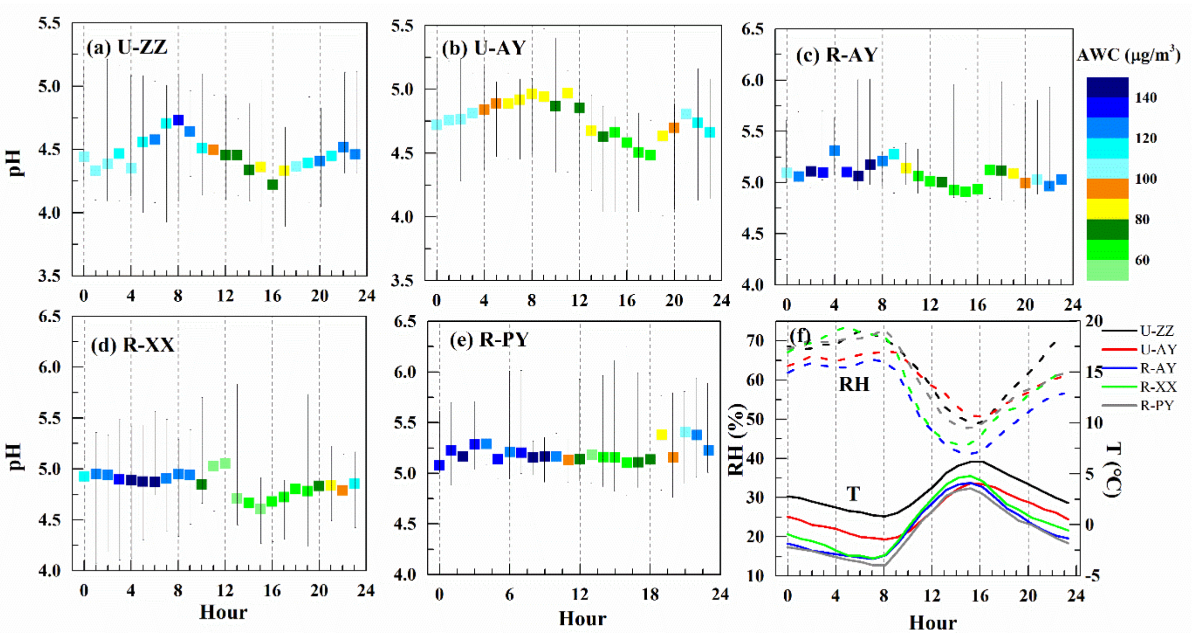

Fig. 4 (a)–(e) Diurnal patterns of median pH values, (f) average RH, and T of the five sites in Case 2. The upper and lower ends of the line represent the maximum and minimum values of pH, respectively. The color scale bar represents AWC concentration.

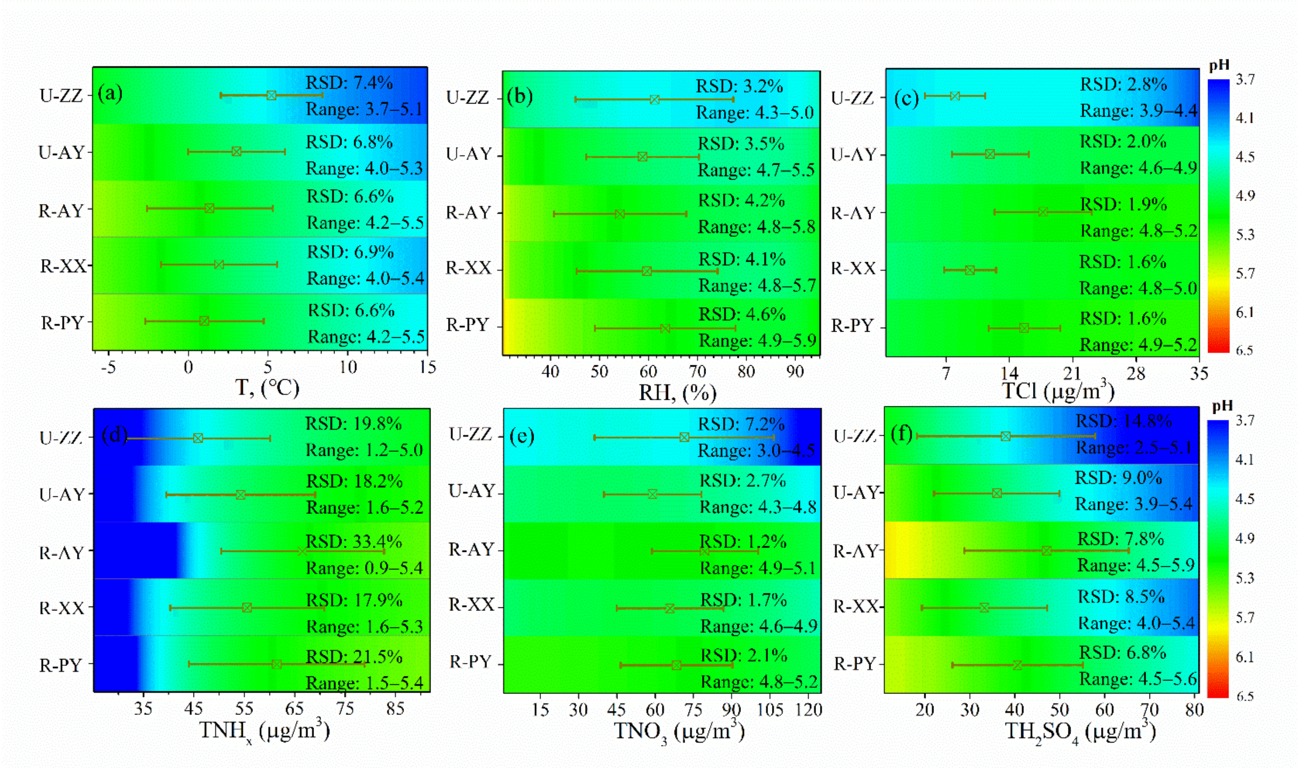

Fig. 5 Comparison of the sensitivities of $PM_{2.5}$ pH to T, RH, TCl ($HCl_{(g)}$ + $Cl_{(aq)}^{-}$), TNH_x ($NH_{3(g)}$ + $NH_{4(aq)}^{+}$), TNO_3 ($HNO_{3(g)}$ + $NO_{3(aq)}^{-}$), and TH_2SO_4 (replaced by observed SO_4^{2-}) among the five sites. A given range for a variable for all sites with corresponding average values of other parameters was used as input to the ISORROPIA-II model. The range of the x-axis is close to the observed minimum and maximum values in Case 2 (Table S4). The color scale bar represents the pH values. The relative standard deviation (RSD) and range (Range) represent the sensitivity degree of pH to this variable and range (min–max) of the re-predicted pH value in the test, respectively. The square plots on the graph represent the average values of each variable observed in Case 2 with standard deviation as an error bar.

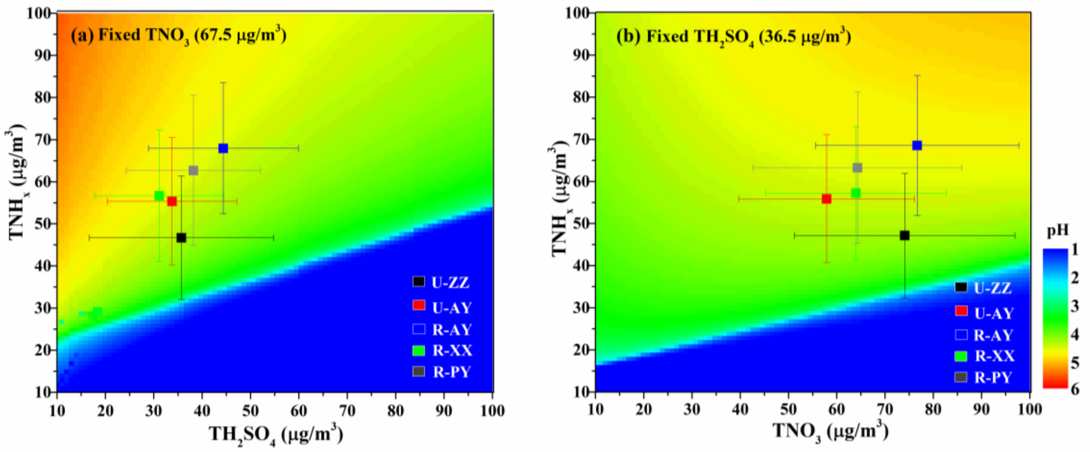

Fig. 6 Particle pH calculated with fixed meteorological parameters (T = 275.5 K and RH = 60 %) under different combinations of TNH$_x$ and (a) TH$_2$SO$_4$ (Fixed TNO$_3$ = 67.5 μg/m^3) and (b) TNO$_3$ (Fixed TH$_2$SO$_4$ = 36.5 μg/m^3). The color scale bar represents the pH values. The markers on the graph represent the average concentrations of TNH$_x$, TH$_2$SO$_4$, and TNO$_3$ at the five sites during Case 2 with standard deviation as error bar.

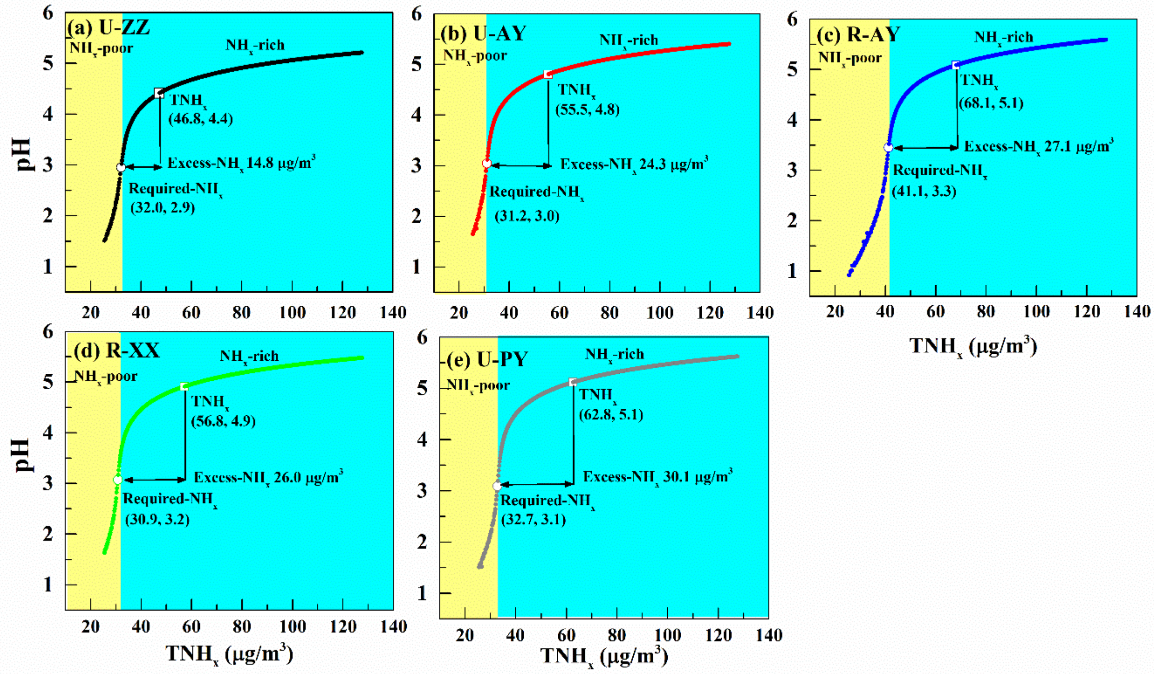

Fig. 7 Particle pH corresponds to increasing TNH$_x$ at the five sites to examine the effects of major indicators of NH_3 (i.e., TNH$_x$, Required-NH$_x$, and Excess-NH$_x$) on aerosol acidity. Particle pH was calculated by using a wide range of TNH$_x$ (25–130 μg/m^3) and average values of other parameters during Case 2 of each site. The concentrations of TNH$_x$, Required-NH$_x$, and Excess-NH$_x$ with corresponding pH values are marked by a hollow box, hollow circle, and arrow respectively. The yellow and blue background colors correspond to the NH$_x$-poor and NH$_x$-rich, respectively.

Table lists:

Table 1 Comparison of the particle pH values in this study (median, min–max) and other sites (mean ± standard deviation).

Table 2 Descriptions of the five sampling sites.

Table 3 Summary (mean ± standard deviation) of gaseous precursors (μg/m^3), water-soluble inorganic ions (μg/m^3), T (°C), and RH (%) during three cases of haze periods at five monitoring sites.

Table 4 Sensitivity of pH to input data. The real-time measured values of a variable and the average values of other parameters during Case 2 were input into the ISORROPIA II. The degree of sensitivity was represented as the relative standard deviation (%RSD) of the re-calculated pH values, higher RSD implied higher sensitivity of this factor to pH and thus is more important for local pH.

Table 1 Comparison of the particle pH values in this study (median, min–max) and other sites (mean ± standard deviation).

	Observation site	Period	pH	Model	Reference
This study	Zhengzhou, China (Urban)	Jan 2018	4.5 (3.8–5.2)	ISORROPIA-II	
	Anyang, China (Urban)	Jan 2018	4.8 (3.9–5.8)		
	Anyang, China (Rural)	Jan 2018	4.9 (4.1–6.2)		
	Xinxiang, China (Rural)	Jan 2018	5.1 (4.7–6.3)		
	Puyang, China (Rural)	Jan 2018	5.2 (4.8–6.5)		
China	Beijing, China (Urban)	Feb 2017	4.5 ± 0.7	ISORROPIA-II	Ding et al., 2019
	Beijing, China (Urban)	Dec 2016	4.3 ± 0.4	ISORROPIA-II	Liu et al., 2017
	Beijing, China (Urban)	Jan–Feb 2015	4.5	ISORROPIA-II	Guo et al., 2017
	Xi'an, China (Urban)	Nove–Dec 2012	5.0	ISORROPIA-II	Guo et al., 2017
	Tianjin, China (Urban)	Dec–Jun 2015	4.9 ± 1.4	ISORROPIA-II	Shi et al., 2017
	Tianjin, China (Urban)	Aug 2015	3.4 ± 0.5	ISORROPIA-II	Shi et al., 2019
	Hohhot, China	Winter 2015	5.7	ISORROPIA-II	Wang et al., 2019
	PRD, China (Rural)	Fall-winter season 2012	0.81 ± 0.24	AIM-II model	Fu et al., 2015
	Hong Kong, China (Urban)	2001	0.25	AIM-II model	Pathak et al., 2004
Other countries	Singapore (Urban)	Sep–Nov 2011	0.60	AIM-IV model	Sailesh et al., 2013
	Northeastern US (Urban)	Feb–Mar 2015	0.07 ± 0.96	ISORROPIA-II	Guo et al., 2016
	Alabama, USA (Rural)	Jun–Jul 2013	1.94 ± 0.59	ISORROPIA-II	Guo et al., 2015
	Georgia, USA (Rural)	Aug–Oct 2016	2.2 ± 0.6	ISORROPIA-II	Nah et al., 2018
	Crete, Greece (Background)	Aug–Nov 2012	1.25 ± 1.14	ISORROPIA-II	Boucher et al., 2016

Table 2 Descriptions of the five sampling sites.

City	Classification	Site	Coordinate	Location	Surrounding environment	Emission (Gg)		
						NH_3[*]	SO_2[**]	NO_x[**]
Zhengzhou	Urban	U-ZZ	34.82° N 113.54° E	West to the Zhengzhou downtown (Zhengzhou University)	Densely occupied residences, light industry, freeways and roads	39.2	36.7	31.8
Anyang	Urban	U-AY	36.09° N 114.41° E	East to the Anyang downtown (Anyang Environmental Protection Bureau)	Occupied residences, heavy industry and traffic roads	57.8	46.9	37.1
	Rural	R-AY	36.22° N 114.39° E	15 km north of Anyang city (Baizhuang town)	High ways, small villages, and cropland			
Xinxiang	Rural	R-XX	35.38° N 114.30° E	35 km northeast of Xinxiang city (Banzao town)	Small villages and cropland	72.1	8.9	19.6
Puyang	Rural	R-PY	36.15° N 115.10° E	44 km north of Puyang city (Liangcun town)	Small villages and cropland	39.6	3.4	3.2

[*] Data from a 2015-based NH_3 emission inventory (Wang et al., 2018a).

[**] Data from Henan Statistical Yearbook of 2018 (BSH, 2018).

Table 3 Summary (mean ± standard deviation) of gaseous precursors (μg/m^3), water-soluble inorganic ions (μg/m^3), T (°C), and RH (%) during three cases of haze periods at five sites.

	Case 1 (January 12−14)					Case 2 (January 14−21)					Case 3 (January 21−25)				
	U-ZZ	U-AY	R-AY	R-XX	R-PY	U-ZZ	U-AY	R-AY	R-XX	R-PY	U-ZZ	U-AY	R-AY	R-XX	R-PY
HNO_3	0.9 ± 0.2	0.7 ± 0.2	3.1 ± 0.2	3.0 ± 0.1	3.9 ± 0.1	1.3 ± 0.3	1.1 ± 0.3	3.7 ± 0.4	3.7 ± 0.5	4.2 ± 0.2	0.9 ± 0.3	0.7 ± 0.2	4.9 ± 1.0	3.3 ± 0.2	3.3 ± 0.2
NH_3	17.0 ± 3.7	19.6 ± 8.0	22.9 ± 6.3	21.6 ± 4.1	17.8 ± 3.7	19.5 ± 5.2	23.6 ± 6.5	25.2 ± 6.5	24.7 ± 9.9	26.5 ± 6.7	10.5 ± 6.9	8.8 ± 4.7	10.6 ± 4.7	8.4 ± 3.5	12.1 ± 3.5
HCl	0.1 ± 0.0	0.7 ± 0.6	0.5 ± 0.1	0.6 ± 0.1	1.8 ± 0.1	0.1 ± 0.1	0.4 ± 0.1	0.6 ± 0.2	0.6 ± 0.1	2.0 ± 0.1	0.1 ± 0.1	0.5 ± 0.1	1.7 ± 0.1	1.0 ± 0.4	1.5 ± 0.4
NO_3^-	41.5 ± 14.6	28.0 ± 14.6	43.0 ± 12.5	32.8 ± 12.9	25.2 ± 9.1	74.2 ± 32.9	58.0 ± 18.3	76.8 ± 21.1	64.1 ± 18.7	64.4 ± 21.7	32.4 ± 13.5	18.9 ± 5.4	26.0 ± 5.8	25.1 ± 6.7	18.8 ± 4.3
NH_4^+	18.6 ± 6.2	15.9 ± 8.3	21.8 ± 8.0	14.9 ± 6.2	12.8 ± 4.5	31.9 ± 12.5	35.2 ± 12.0	47.6 ± 13.1	35.6 ± 10.4	39.9 ± 14.9	17.4 ± 6.0	11.6 ± 4.4	14.3 ± 4.4	12.9 ± 4.0	10.1 ± 2.9
SO_4^{2-}	17.8 ± 7.2	14.4 ± 9.0	13.7 ± 10.0	10.0 ± 5.5	8.6 ± 2.3	38.3 ± 18.0	34.5 ± 13.0	46.8 ± 16.9	32.9 ± 12.5	39.2 ± 13.6	19.8 ± 8.6	15.1 ± 6.1	15.1 ± 7.3	14.4 ± 4.8	13.3 ± 4.0
Ca^{2+}	0.7 ± 0.5	0.5 ± 0.3	5.0 ± 2.2	0.8 ± 0.2	3.4 ± 0.3	0.5 ± 0.4	0.4 ± 0.4	2.2 ± 1.2	1.0 ± 0.3	3.3 ± 0.6	0.1 ± 0.1	0.2 ± 0.2	1.8 ± 0.7	0.5 ± 0.1	2.4 ± 0.5
Na^+	1.5 ± 0.2	1.0 ± 0.0	1.4 ± 0.4	0.7 ± 0.1	2.2 ± 0.1	1.6 ± 0.2	1.0 ± 0.1	1.4 ± 0.4	0.8 ± 0.1	2.2 ± 0.0	1.1 ± 0.2	1.0 ± 0.2	2.2 ± 0.4	1.3 ± 0.4	2.2 ± 0.2
Cl^-	7.5 ± 2.5	2.7 ± 3.4	6.6 ± 2.5	5.4 ± 1.5	6.3 ± 1.2	8.5 ± 3.2	12.0 ± 4.2	18.5 ± 5.0	9.7 ± 2.6	14.4 ± 3.8	3.3 ± 1.5	4.5 ± 1.6	6.9 ± 1.6	4.7 ± 0.9	5.4 ± 1.4
Mg^{2+}	0.2 ± 0.0	0.1 ± 0.0	0.4 ± 0.1	0.1 ± 0.0	0.5 ± 0.0	0.2 ± 0.0	0.1 ± 0.0	0.4 ± 0.4	0.1 ± 0.0	0.5 ± 0.1	0.2 ± 0.0	0.1 ± 0.0	0.4 ± 0.1	0.1 ± 0.1	0.4 ± 0.1
K^+	2.9 ± 0.7	1.4 ± 0.5	1.6 ± 0.6	1.6 ± 0.4	2.5 ± 0.6	4.4 ± 1.7	2.4 ± 0.7	2.9 ± 0.7	1.9 ± 0.6	3.7 ± 1.1	1.9 ± 0.7	0.9 ± 0.3	0.8 ± 0.3	0.8 ± 0.2	1.2 ± 0.4
T	0.3 ± 3.1	−0.9 ± 3.7	−1.8 ± 4.4	−2.0 ± 3.9	−1.7 ± 4.8	4.2 ± 2.2	2.6 ± 2.5	0.1 ± 2.8	1.2 ± 2.9	0.4 ± 3.0	−0.8 ± 1.8	−2.7 ± 1.8	−3.2 ± 1.9	−2.8 ± 2.6	−4 ± 2.3
RH	63.7 ± 12.1	60.3 ± 15.4	54.0 ± 16.0	58.5 ± 13.5	49.7 ± 14.5	66.0 ± 11.4	60.1 ± 9.9	58.6 ± 9.9	62.7 ± 11.6	65.8 ± 11.7	67 ± 13.1	63.7 ± 13.8	55.9 ± 13.6	59 ± 13.7	56.8 ± 16

Table 4 Sensitivity of pH to input data. The real-time measured values of a variable and the average values of other parameters during Case 2 were input into the ISORROPIA II. The degree of sensitivity was represented as the relative standard deviation (%RSD) of the re-calculated pH values, higher RSD implied higher sensitivity of this factor to pH and thus is more important for local pH.

	TH_2SO_4	TNH_x	TNO_3	TNa	TCl	Ca^{2+}	K^+	Mg^{2+}	RH	T
U-ZZ	12.1 %	12.8 %	6.1 %	0.1 %	0.3 %	3.3 %	0.3 %	0.2 %	1.3 %	2.7 %
U-AY	5.8 %	7.4 %	1.0 %	0.1 %	1.1 %	0.4 %	0.3 %	0.0 %	1.6 %	2.8 %
R-AY	6.5 %	10.9 %	1.4 %	0.1 %	0.7 %	1.2 %	0.2 %	0.3 %	1.9 %	2.7 %
R-XX	5.4 %	11.1 %	1.1 %	0.1 %	0.7 %	0.4 %	0.2 %	0.1 %	2.0 %	2.9 %
R-PY	4.7 %	9.4 %	1.5 %	0.0 %	0.7 %	0.5 %	0.4 %	0.1 %	2.3 %	3.1 %

Supplement materials:

Text S1 Calculation of ions balance and equivalent ratio.

Text S2 Backward trajectory frequency analysis

Text S3 NH_x calculation

Text S1 Calculation of ions balance and equivalent ratio.

The ions balance and equivalent ratio are calculated using the following formulas:

$$[\text{cations}] = \frac{[NH_4^+]}{18} + \frac{[Na^+]}{23} + \frac{[K^+]}{39} + \frac{[Ca^{2+}]}{20} + \frac{[Mg^{2+}]}{12} \tag{1}$$

$$[\text{anions}] = \frac{[SO_4^{2-}]}{48} + \frac{[NO_3^-]}{62} + \frac{[Cl^-]}{35.5} \tag{2}$$

$$\text{ion balance} = [\text{cations}] - [\text{anions}] \tag{3}$$

$$\text{equivalent ratio} = [\text{cations}]/[\text{anions}] \tag{4}$$

where $[Na^+]$, $[K^+]$, $[Ca^{2+}]$, $[Mg^{2+}]$, $[NH_4^+]$, $[SO_4^{2-}]$, $[NO_3^-]$, and $[Cl^-]$ are the measured concentrations (μg/m^3) in the atmosphere. In addition to the measurement uncertainties, equivalent ratios lower than 1 might be attributed to the loss of cations from the volatilization of ammonium and unmeasured hydrogen ions (Meng et al., 2016). Equivalent ratios higher than 1 were most likely caused by water-soluble organic anions, CO_3^{2-} and HCO_3^- contents that were not detected in chemical analysis (Tian et al., 2018).

Text S2 Backward trajectory frequency analysis

The Hybrid Single-Particle Lagrangian Integrated Trajectory (HYSPLIT) Web version of the

National Oceanic and Atmospheric Administration Air Resources Laboratory (Stein et al., 2015) was used to calculate backward trajectories from gridded meteorological data (at 500 m above ground level) at regular time intervals (12 h). For modeling the trajectory frequency, the system will start a trajectory from a single location and height every 6 hours and then sum the frequency that the trajectory passed over a grid cell and then normalize by either the total number of trajectories or endpoints. The grid resolution was selected as 1° according to the scale of the desired result. The frequency distribution maps (Fig. S7) of the five sampling sites recorded during the three cases support our findings: the southern regions of Henan Province (e.g., Xuchang and Zhumadian cities) were a high probability (> 20 %) source for the five sites during Case 1 (Fig. S7a); the trajectory frequency during Case 2 (Fig. S7b) uniformly distributed around the receptor sites is most probably connected to local emissions; and the five sites during Case 3 (Fig. S7c) were affected by the air masses from northeastern areas (e.g., Dezhou and Liaocheng cities) with the frequencies higher than 20 %.

Text S3 NH_x calculation

With respect to measurements of semi-volatile gases, the concentrations of NH_3 were extremely higher than HNO_3 and HCl, consistent with the Song et al. (2018) and Liu et al. (2017). TNHx, required NHx (Required-NHx), and excess NHx (Excess-NHx) concentrations were calculated using the following formulas:

$$\text{Total NH}_x = 17 \times \left(\frac{[\text{NH}_4^+]}{18} + \frac{[\text{NH}_3]}{17}\right), \quad (5)$$

$$\text{Required NH}_x = 17 \times \left(\frac{[\text{SO}_4^{2-}]}{48} + \frac{[\text{NO}_3^-]}{63} + \frac{[\text{Cl}^-]}{35.5} + \frac{[\text{HNO}_3]}{64} + \frac{[\text{HCl}]}{36.5}\right) - 17 \times \left(\frac{[\text{Na}^+]}{23} + \frac{[\text{K}^+]}{39} + \frac{[\text{Ca}^{2+}]}{20} + \frac{[\text{Mg}^{2+}]}{12}\right), \quad (6)$$

$$\text{Excess NH}_x = \text{total NH}_x - \text{required NH}_x, \quad (7)$$

where [Na^+], [K^+], [Ca^{2+}], [Mg^{2+}], [NH_4^+], [SO_4^{2-}], [NO_3^-], [Cl^-], [NH_3], [HNO_3], and [HCl] are the measured mass concentrations (μg/m^3) of these species. Excess-NH$_x$ in this study represents a part of TNH$_x$ (gas NH_3 + particle NH_4^+), while the other NH$_x$ plus nonvolatile cations have been equivalent to all anions (Blanchard et al., 2000). If Excess-NH$_x$ is above 0, then the system is considered NH$_x$-rich. Otherwise, the system is under the NH$_x$-poor condition.

Figure lists:

Fig. S1 Locations of the five monitoring stations in Henan Province, China (i.e., urban sites at Zhengzhou (U-ZZ) and Anyang (U-AY), rural sites at Anyang (R-AY), Xinxiang (R-XX), and Puyang (R-PY)). © 2019 National Geomatics Center of China. All rights reserved.

Fig. S2 Comparison between the predicted and measured NH_4^+, NO_3^-, Cl^-, NH_3, HNO_3 and HCl at the five sites.

Fig. S3 Ion balance of water-soluble inorganic ions at the five sites.

Fig. S4 Comparison between the predicted and input NH_4^+ (a, d) and NH_3 (b, c) concentrations, the original and adjusted pH (c, f) of U-ZZ and R-PY sites after adjusting the measured NH_4^+ concentrations to fit the ion balance.

Fig. S5 Comparison of predicted pH by ISORROPIA-II with E-AIM IV at the U-ZZ site.

Fig. S6 Temporal variations of temperature (T), relative humidity (RH), wind speed (WS), wind direction (WD), and concentrations of NH_3, NH_4^+, SO_4^{2-}, and NO_3^- during three cases at U-AY (a), R-

AY (b), R-XX (c), and R-PY (d) sites. The shaded areas represent the measurement uncertainties.

Fig. S7 Trajectory frequencies of typical periods at the five sites during Cases 1(a), 2(b), and 3(c). The color scale bar represents the percentage of trajectories passing through each grid to total trajectories.

Fig. S8 Time series of predicted PM$_{2.5}$ pH at the five sites. The shaded areas show the range of uncertainty in pH for the pH$_{max}$ and pH$_{min}$ calculations.

Fig. S9 Correlations between pH and H^+_{air} during sampling periods at the five sites. The color scale bar represents the aerosol water content (AWC) concentration.

Fig. S10 Sensitivity tests of PM$_{2.5}$ pH to input data. The real-time measured values of a variable and the average values of other parameters during Case 2 were input into the ISORROPIA II model.

Fig. S11 Comparisons of the sensitivities of PM$_{2.5}$ pH to TNa, K^+, Ca^{2+}, and Mg^{2+} among the five sites. The color scale bar represents the pH values. The relative standard deviation (RSD) and range (Range) represent the sensitivity degree of pH to this variable and range (min–max) of the re-predicted pH value in the test, respectively.

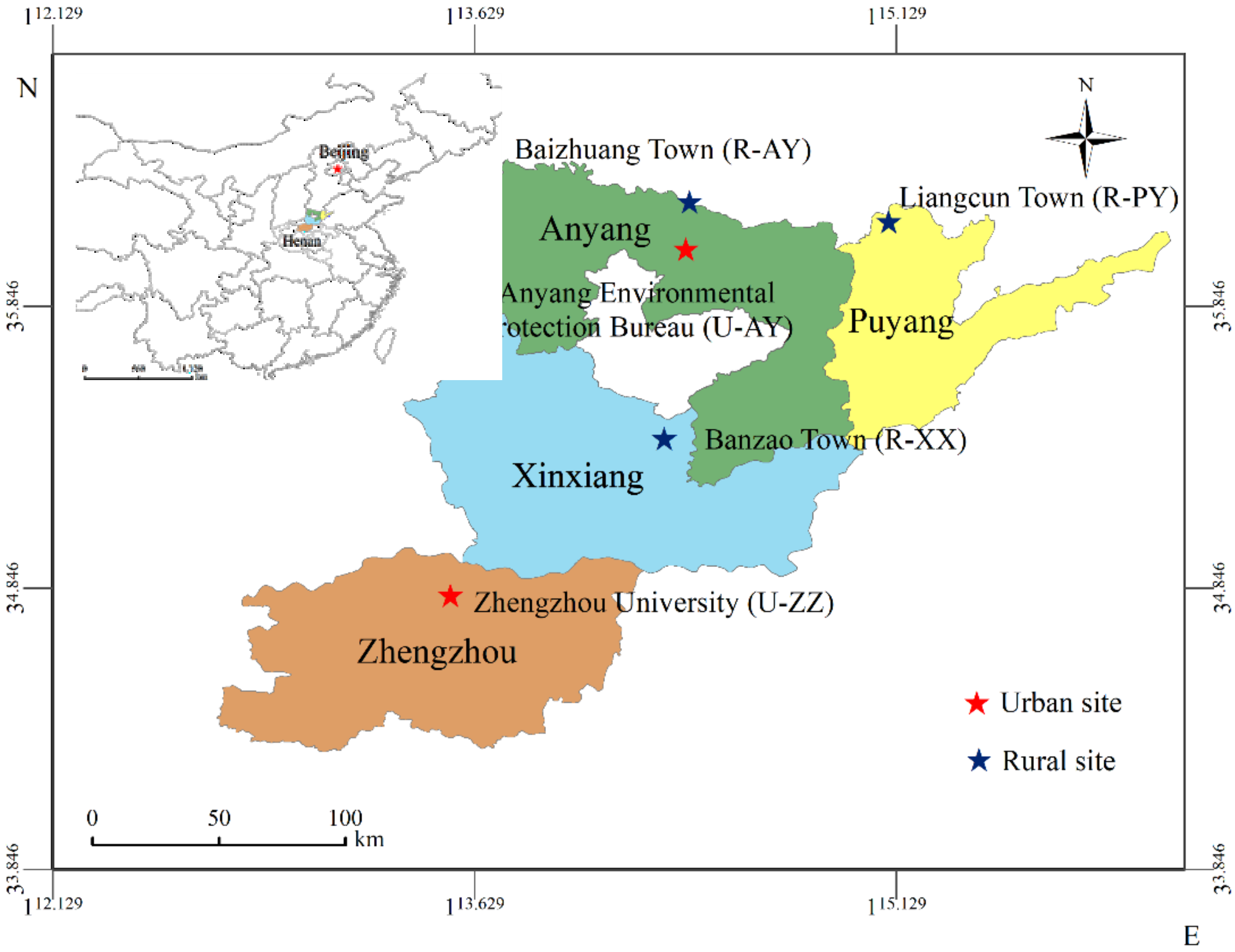

Fig. S1 Locations of the five monitoring stations in Henan Province, China (i.e., urban sites at Zhengzhou (U-ZZ) and Anyang (U-AY), rural sites at Anyang (R-AY), Xinxiang (R-XX), and Puyang (R-PY)). © 2019 National Geomatics Center of China. All rights reserved.

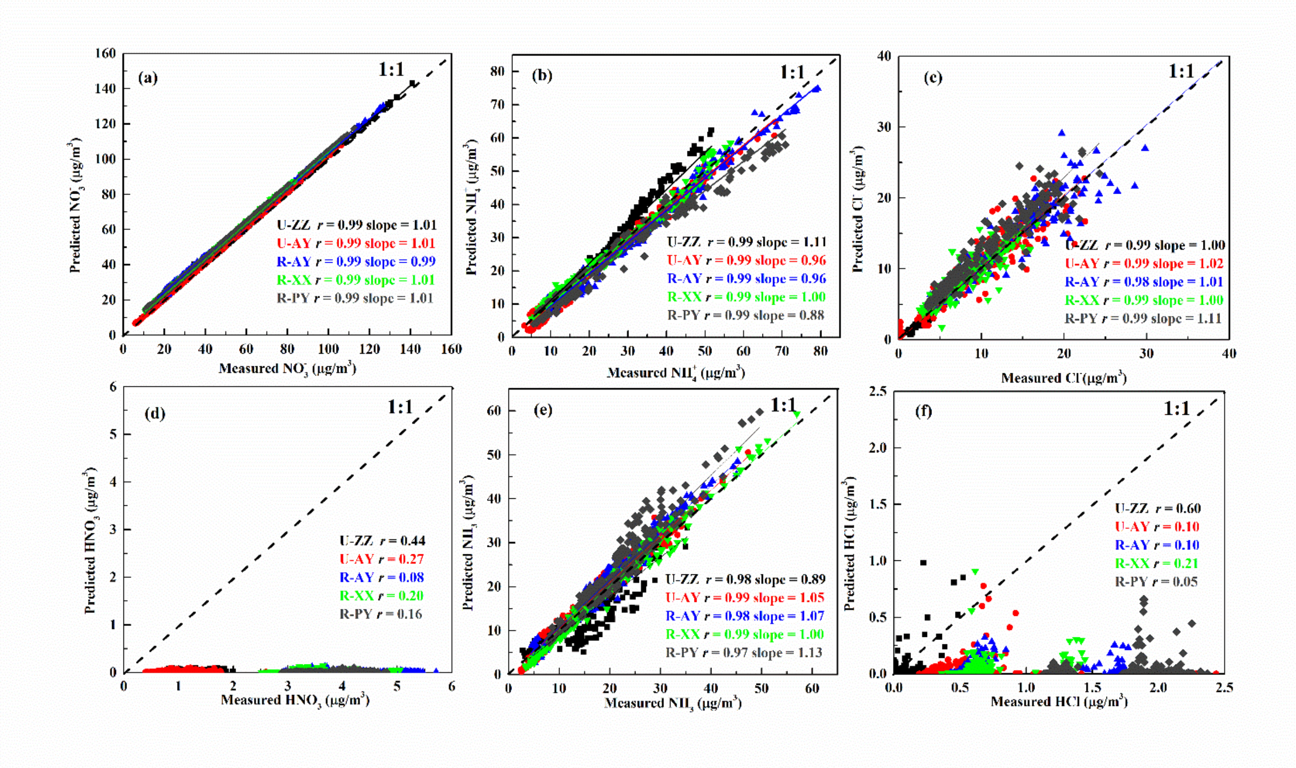

Fig. S2 Comparison between the predicted and measured NH_4^+, NO_3^-, Cl^-, NH_3, HNO_3 and HCl at the five sites.

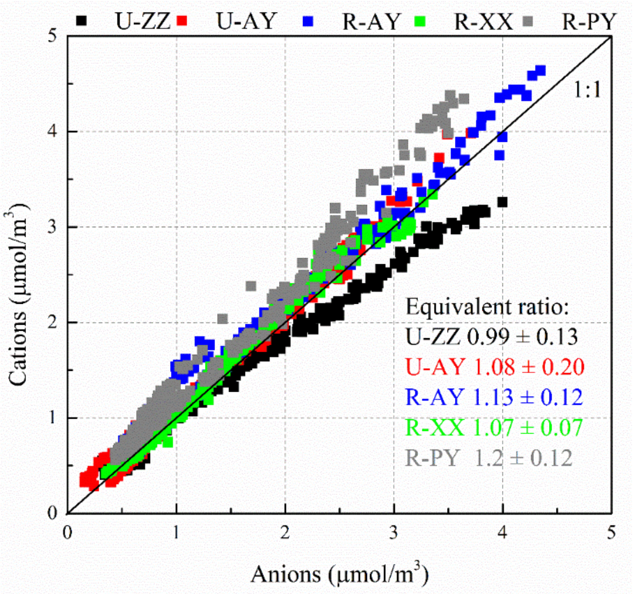

Fig. S3 Ion balance of water-soluble inorganic ions at the five sites.

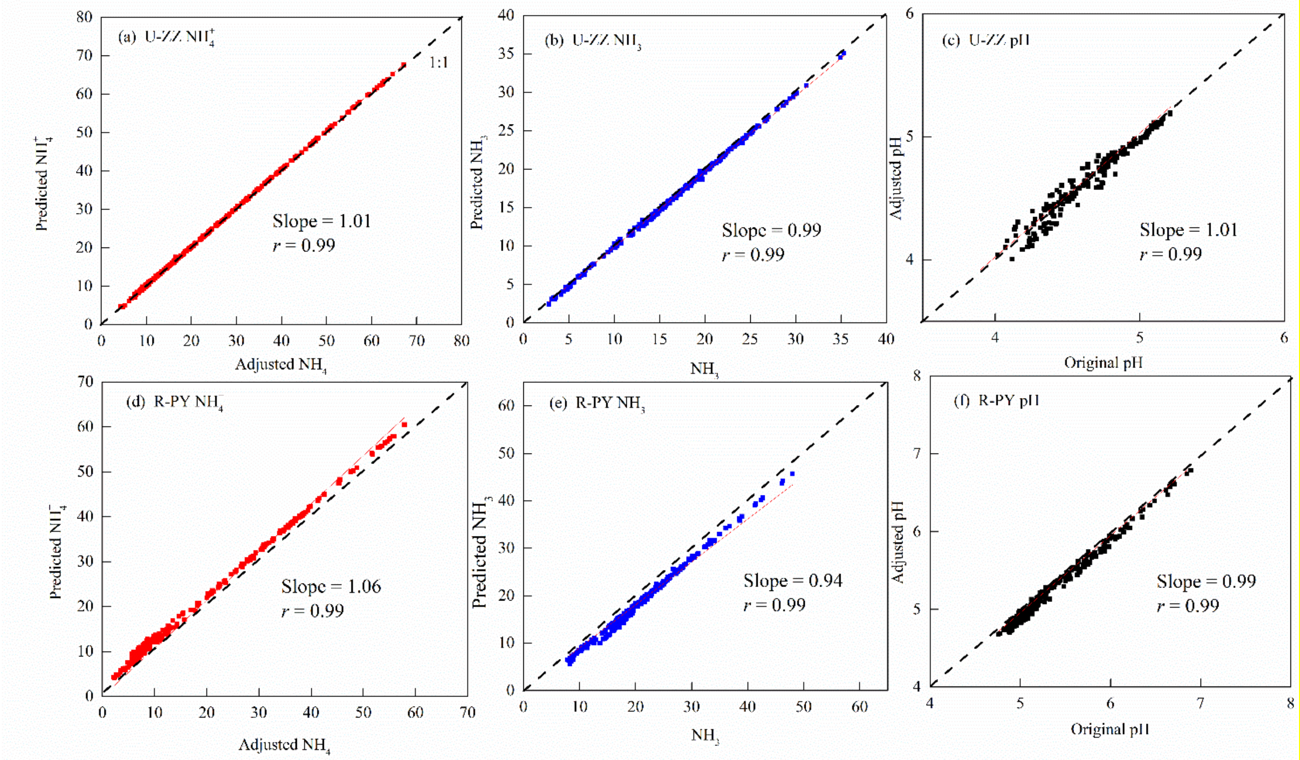

Fig. S4 Comparison between the predicted and input NH_4^+ (a, d) and NH_3 (b, c) concentrations, the original and adjusted pH (c, f) of U-ZZ and R-PY sites after adjusting the measured NH_4^+ concentrations to fit the ion balance.

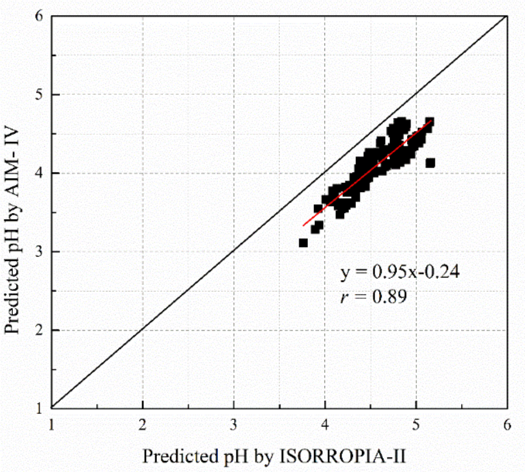

Fig. S5 Comparison of predicted pH by ISORROPIA-II with E-AIM IV at the U-ZZ site.

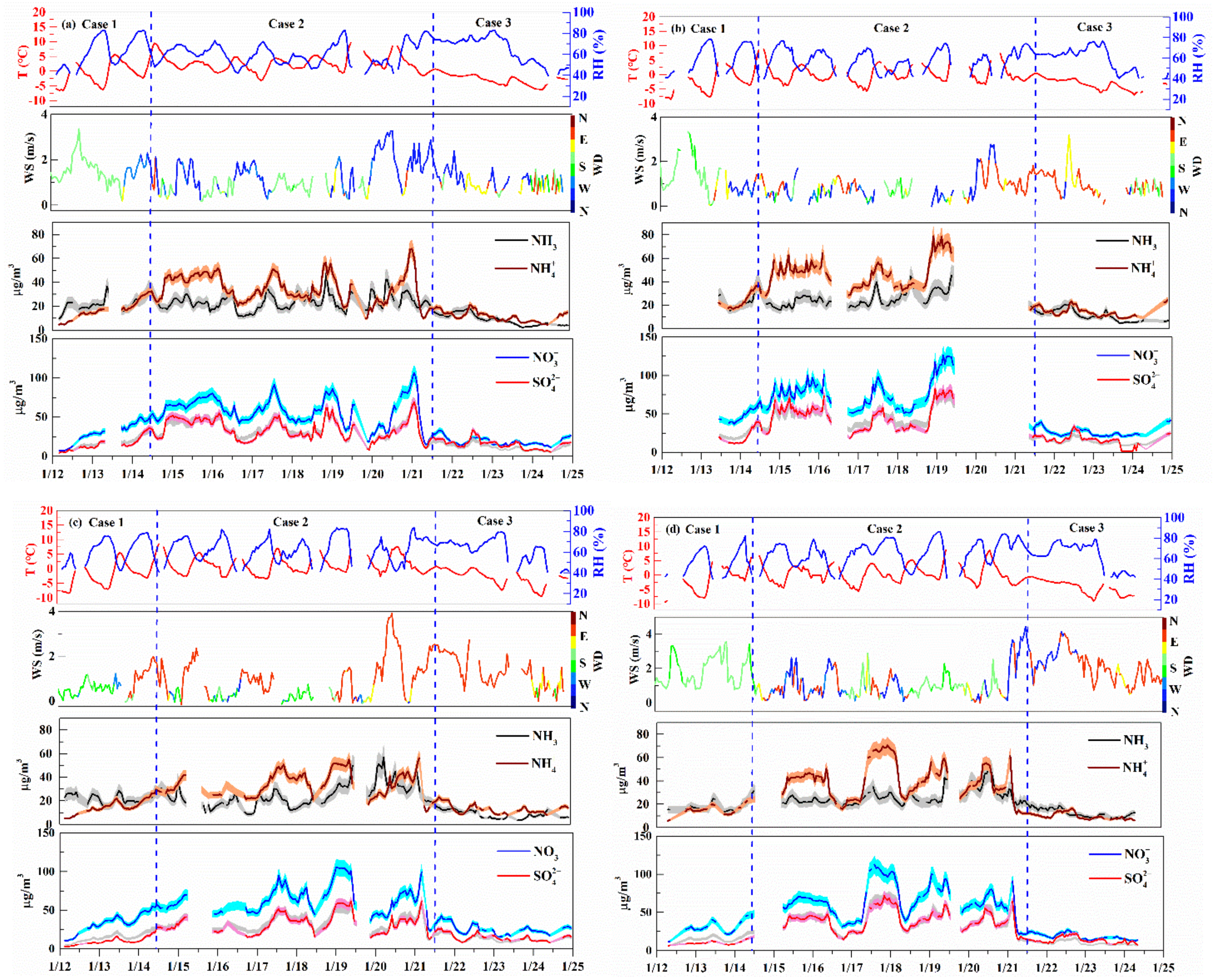

Fig. S6 Temporal variations of temperature (T), relative humidity (RH), wind speed (WS), wind direction (WD), and concentrations of NH_3, NH_4^+, SO_4^{2-}, and NO_3^- during three cases at U-AY (a), R-AY (b), R-XX (c), and R-PY (d) sites. The shaded areas represent the measurement uncertainties.

(a) Case 1

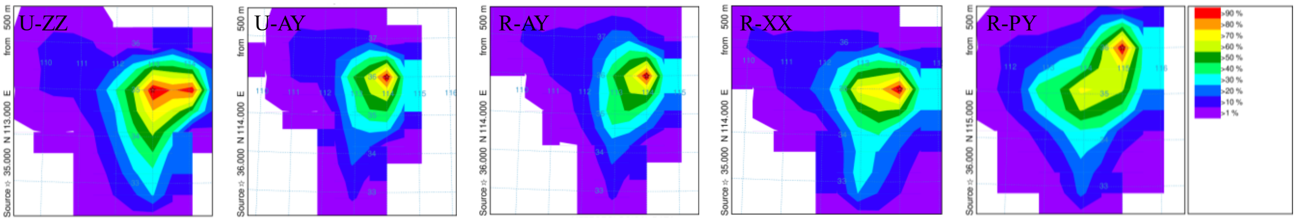

(b) Case 2

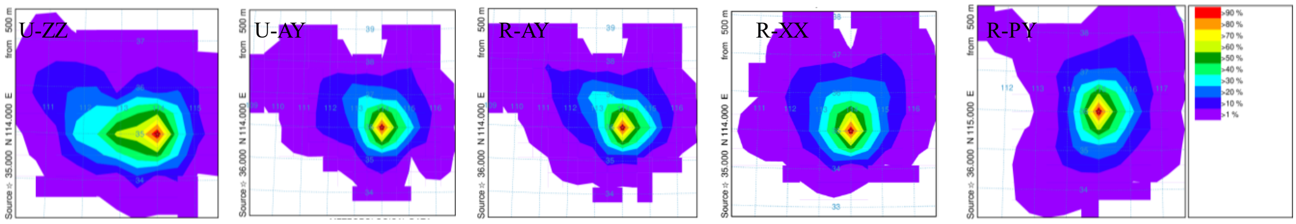

(c) Case 3

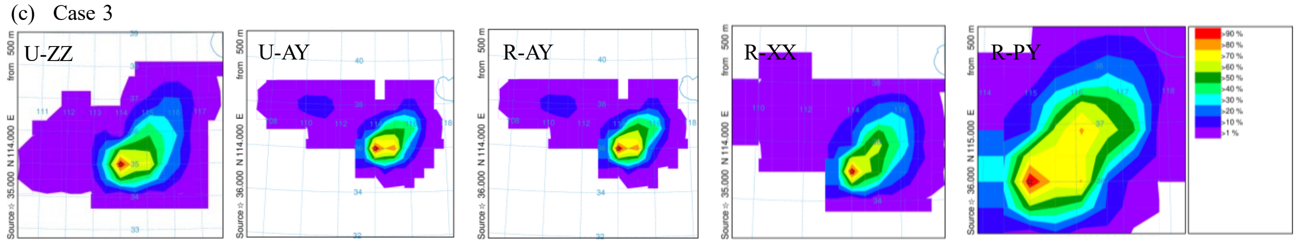

Fig. S7 Trajectory frequencies of typical periods at the five sites during Cases 1(a), 2(b), and 3(c). The color scale bar represents the percentage of trajectories passing through each grid to total trajectories.

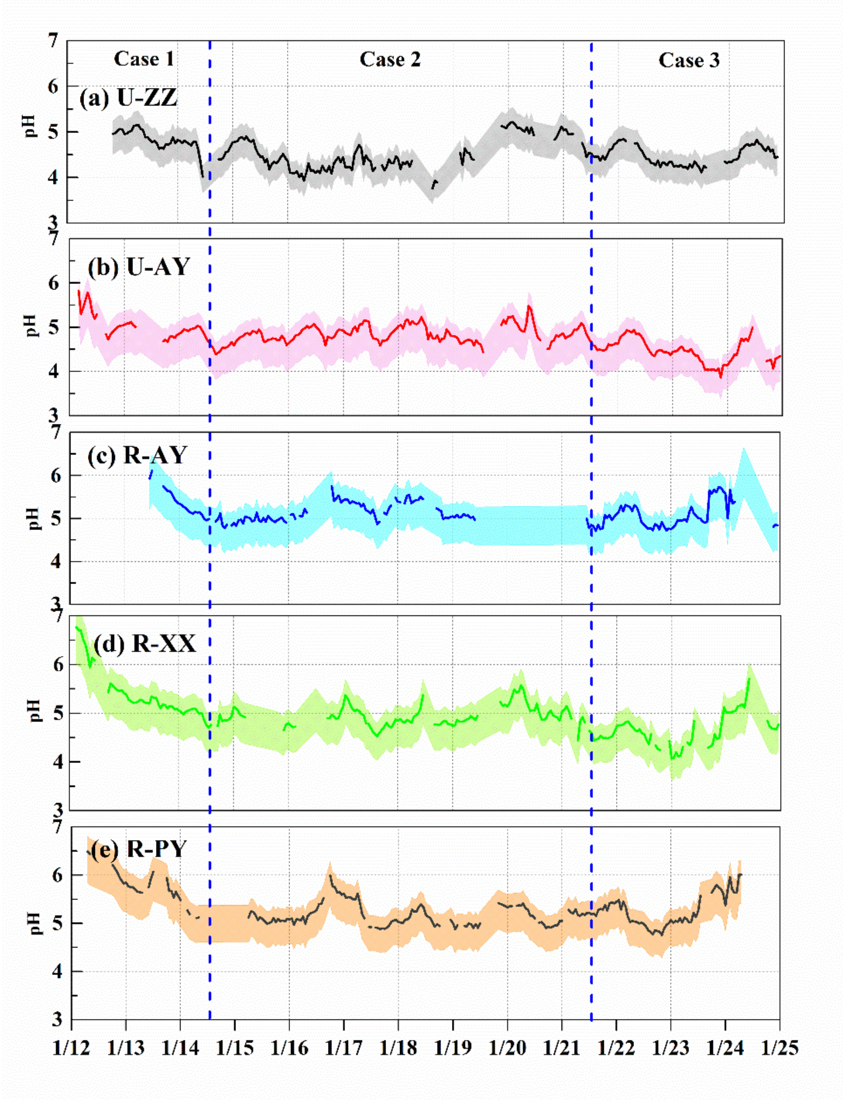

Fig. S8 Time series of predicted $PM_{2.5}$ pH at the five sites. The shaded areas show the range of uncertainty in pH for the pH_{max} and pH_{min} calculations.

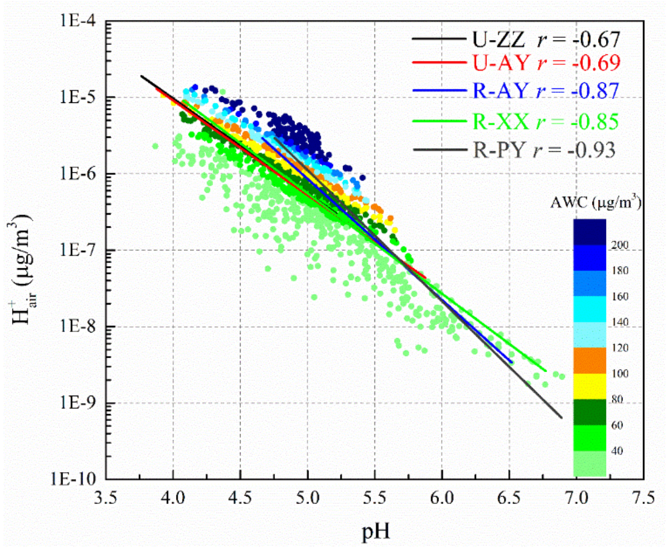

Fig. S9 Correlations between pH and H^+_{air} during sampling periods at the five sites. The color scale bar represents the aerosol water content (AWC) concentration.

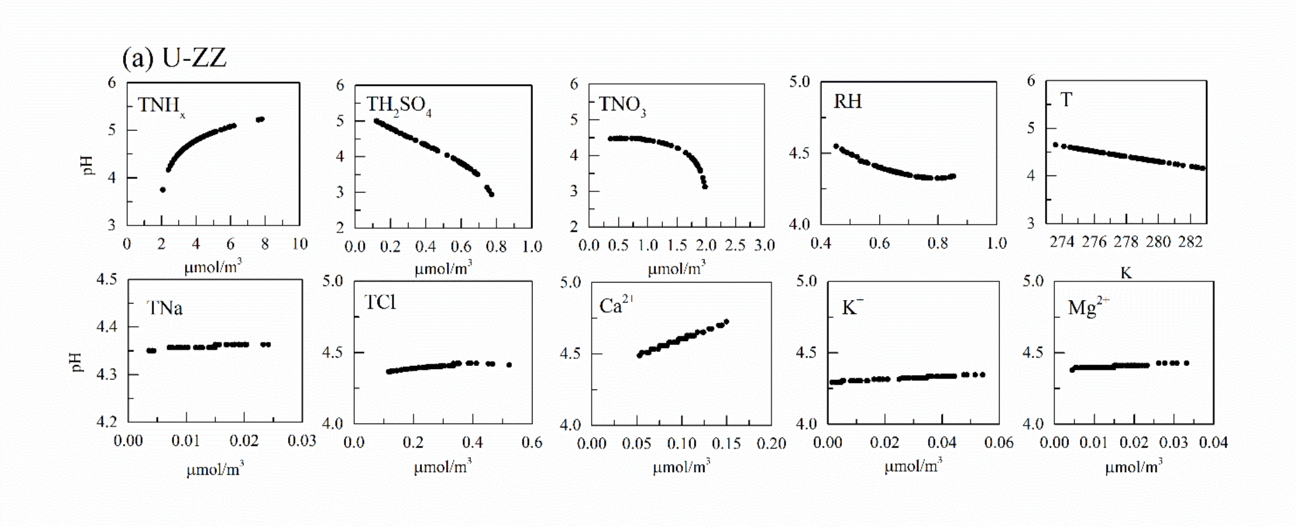

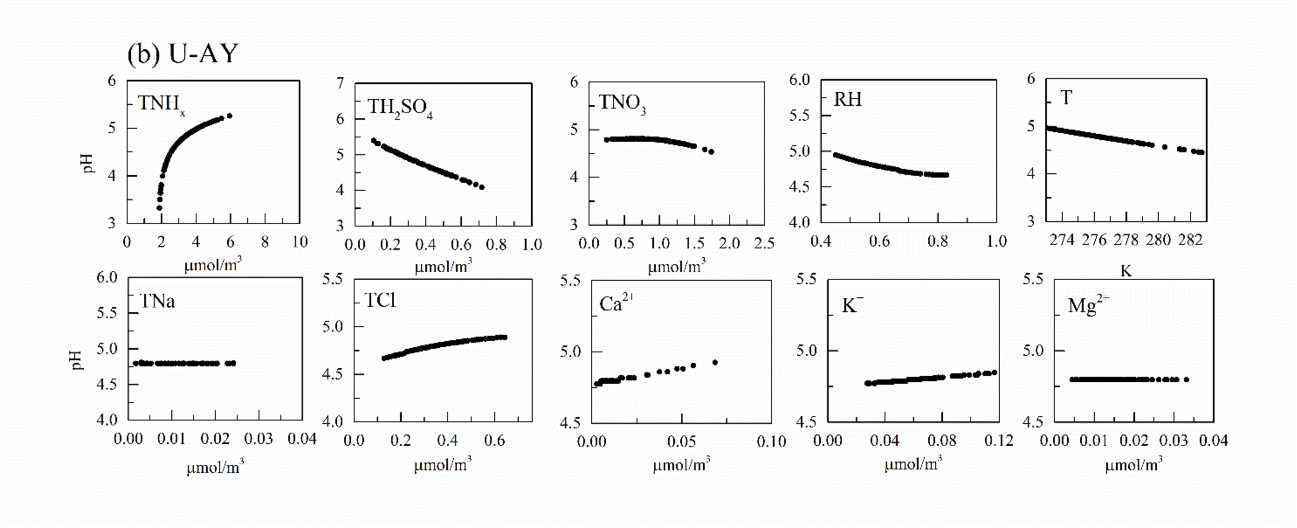

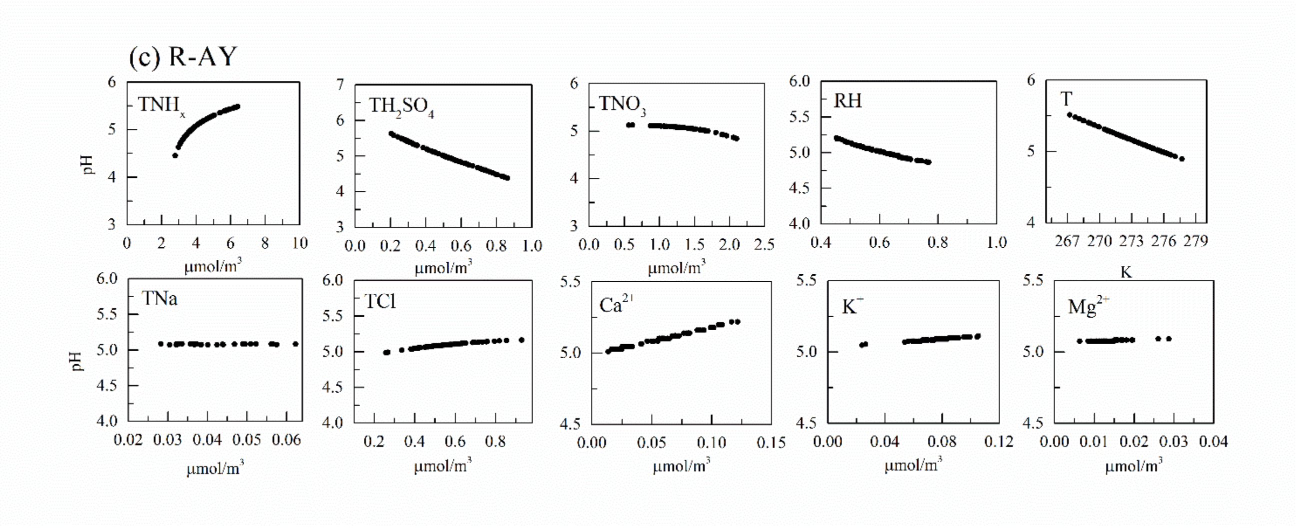

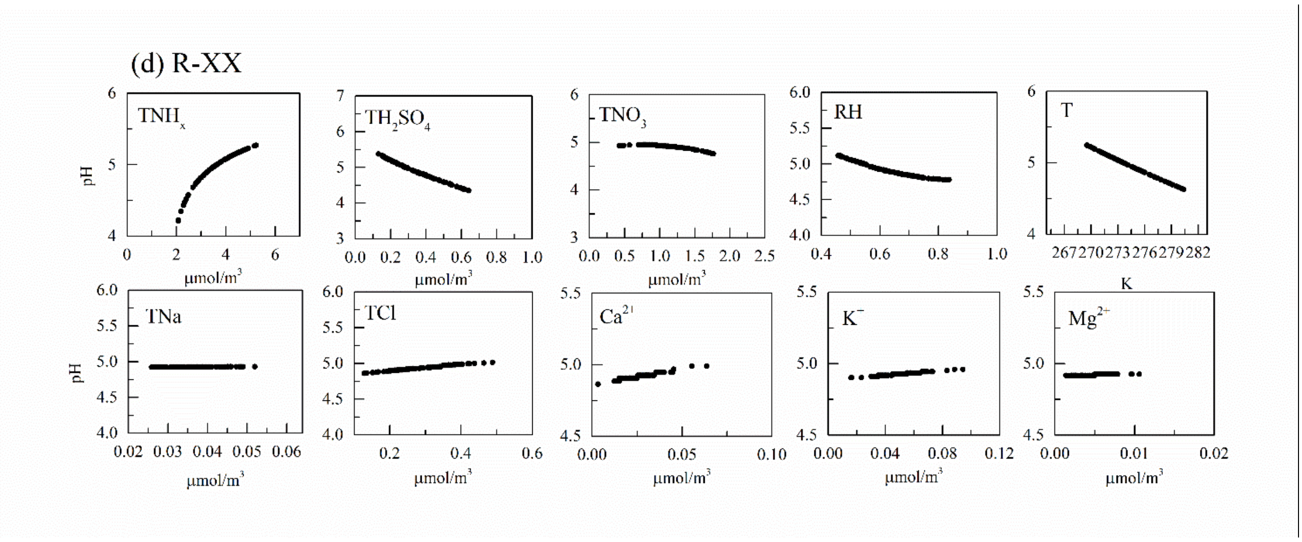

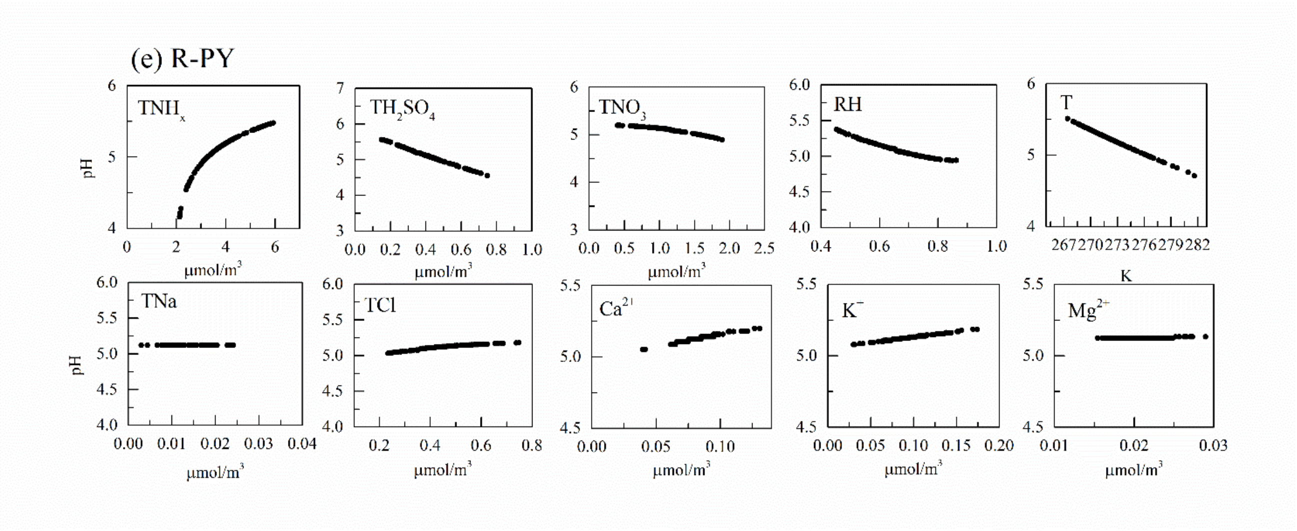

Fig. S10 Sensitivity tests of $PM_{2.5}$ pH to input data. The real-time measured values of a variable and the average values of other parameters during Case 2 were input into the ISORROPIA II model.

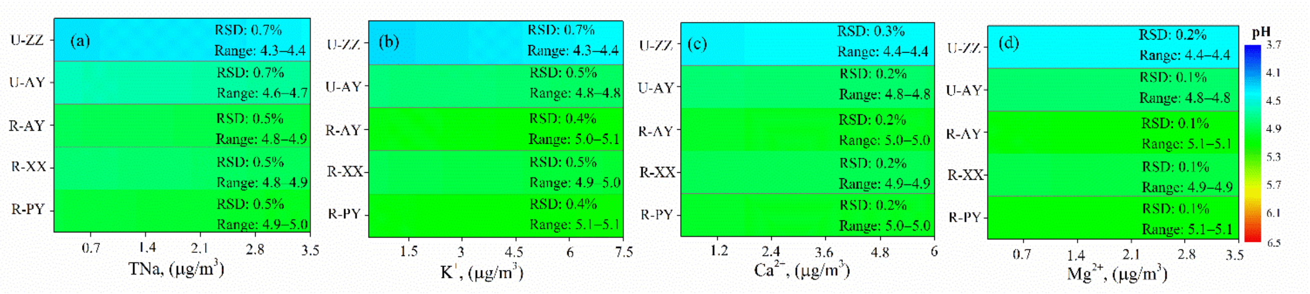

Fig. S11 Comparisons of the sensitivities of $PM_{2.5}$ pH to TNa (replaced by observed Na^+), K^+, Ca^{2+}, and Mg^{2+} among the five sites. The color scale bar represents the pH values. The relative standard deviation (RSD) and range (Range) represent the sensitivity degree of pH to this variable and range (min–max) of the re-predicted pH value in the test, respectively.

Table lists:

Table S1 Summarized NH_3 concentrations (μg/m^3) in this study and other sites.

Table S2 Statistical values of pH during three cases.

Table S3 Pearson's correlation coefficients (*r*) between H^+_{air} with observed data at the five sites.

Table S4 Variation ranges of each variable for assessing the different effects of this variable among five sites and their observed minimum and maximum values.

Table S1 Summarized NH_3 concentrations (μg/m^3) in this study and other sites.

Cities	Period	NH_3	References
Zhengzhou, China	2018.01	22.0 ±8.9	This study
Anyang, China	2018.01	25.3 ± 10.5	This study
Anyang, China	2018.01	25.8 ± 12.0	This study
Xinxiang, China	2018.01	26.1 ± 14.0	This study
Puyang, China	2018.01	27.1 ± 17.3	This study
Zhengzhou, China	2017.03–2018.04	11.7	Wang et al., 2018
Beijing, China	2015.01–03	7.3	Zhang et al., 2018
Beijing, China	2008.02–2010.07	22.8 ± 16.3	Wang et al., 2018
Beijing, China	2007.01–2010.07	10.2 ± 10.8	Wang et al., 2018
Beijing, China	2001.07–2001.08	16.8–42.2	Wang et al., 2018
North China Plain, China	2006.08–2009.09	11.7–31.9	Shen et al., 2011
Xi'an, China	2006.04–2007.04	18.6	Wang et al., 2018
Xi'an, China	2006.04–2007.04	20.3	Wang et al., 2018
Chengdu, China	2014.07–2015.04	10.5 ± 4.8	Wang et al., 2016
Wanzhou, China	2014.07–2015.04	8.3 ± 4.7	Wang et al., 2016
shanghai, China	2014.05–2015.06	7.8	Chang et al., 2019
Hangzhou, China	2012.04–05	12.8	Jansen et al., 2014
Dalian, China	2010.09–2012.04	1.5	Luo et al., 2014
Fenghua, China	2010.08–2012.05	3.7	Luo et al., 2014
Fujian, China	2015.06–2016.05	21.0 ± 7.9	Wang et al., 2018
Fujian, China	2015.06–2017.03	10.5–13.5	Wu et al., 2018
Hong Kong, China	2003.10–2006.05	10.2	Tanner, 2009
Carolina, USA	2000.01–12	0.4–3.4	Walker et al., 2004
Delhi, India	2013.01–2015.12	25.3 ± 4.6	Saraswati et al., 2019

Table S2 Statistical values of pH during three cases.

	Case 1				Case 2				Case 3			
	25th percentile	Median	75th percentile	Average	25th percentile	Median	75th percentile	Average	25th percentile	Median	75th percentile	Average
U-ZZ	4.7	4.8	5.0	4.8	4.3	4.5	4.8	4.5	4.3	4.5	4.7	4.5
U-AY	4.8	5.0	5.2	5.1	4.7	4.8	5.0	4.8	4.4	4.5	4.8	4.5
R-AY	5.1	5.4	5.8	5.5	5.0	5.1	5.4	5.2	4.9	5.0	5.3	5.1
R-XX	5.1	5.3	5.6	5.4	4.8	4.9	5.1	4.9	4.5	4.7	5.0	4.7
R-PY	5.7	6.0	6.3	6.0	5.0	5.1	5.4	5.2	5.0	5.2	5.4	5.3

Table S3 Pearson's correlation coefficients (*r*) between H^{+}_{air} with observed data at the five sites.

	U−ZZ	U−AY	R−AY	R−XX	R−PY
TWSIIs	0.834^{**}	0.521^{**}	0.676^{**}	0.530^{**}	0.774^{**}
TNH_x	0.650^{**}	0.368^{**}	0.544^{**}	0.301^{**}	0.703^{**}
TH_2SO_4	0.867^{**}	0.625^{**}	0.765^{**}	0.638^{**}	0.811^{**}
TNO_3	0.828^{**}	0.458^{**}	0.607^{**}	0.502^{**}	0.767^{**}
TCl	0.430^{**}	0.406^{**}	0.602^{**}	0.223^{**}	0.419^{**}
K^+	0.757^{**}	0.388^{**}	0.551^{**}	0.138^{*}	0.485^{**}
Ca^{2+}	-0.161^{*}	-0.234^{**}	-0.137^{*}	-0.248^{**}	0.06
TNa	0.306^{**}	−0.095	0.098	0.103	-0.138^{*}
Mg^{2+}	−0.009	−0.027	−0.018	−0.050	0.026
AWC	0.63^{**}	0.739^{**}	0.903^{**}	0.755^{**}	0.938^{**}
T	0.012	0.045	-0.138^{*}	−0.023	0.146^{*}
RH	0.337^{**}	0.610^{**}	0.631^{**}	0.637^{**}	0.658^{**}

* Correlation is significant at the 0.05 level (two-tailed).

** Correlation is significant at the 0.01 level (two-tailed).

Table S4 Variation ranges of each variable for assessing the different effects of this variable among five sites and their observed minimum and maximum values.

Species	Observation		Setting		Gradient
	Min	Max	Min	Max	
T (°C)	−5.8	14.3	−6	15	0.1
RH (%)	26.8	92.3	30	95	0.1
TNH_x ($\mu g/m^3$)	21.2	96.7	25	95	0.01 $\mu mol/m^3$
TNO_3 ($\mu g/m^3$)	5.8	132.6	1	125	0.01 $\mu mol/m^3$
TH_2SO_4 ($\mu g/m^3$)	6.9	82.7	10	80	0.01 $\mu mol/m^3$
TCl ($\mu g/m^3$)	0.54	39.5	0.35	35	0.01 $\mu mol/m^3$
TNa ($\mu g/m^3$)	0.29	3.33	0.25	3.5	0.01 $\mu mol/m^3$
K^+ ($\mu g/m^3$)	0.27	7.8	0.1	7.5	0.01 $\mu mol/m^3$
Ca^{2+} ($\mu g/m^3$)	0.2	5.2	0.4	6	0.01 $\mu mol/m^3$
Mg^{2+} ($\mu g/m^3$)	0.11	3.1	0.25	3.5	0.01 $\mu mol/m^3$

References:

Blanchard, C. L., P. M. Roth, S. J. Tanenbaum, S. D. Ziman, and J. H. Seinfeld: The use of ambient measurements to identify which precursor species limit aerosol nitrate formation, J. Air Waste Manage. Assoc., 50, 2073–2084, 2000.

Chang, Y., Zou, Z., Zhang, Y., Deng, C., Hu, J., Shi, Z., Dore, A. J., Collett, J. L.: Assessing contributions of agricultural and nonagricultural emissions to atmospheric ammonia in a Chinese megacity. Environ. Sci. Technol., 53, 1822–1833, 2019.

Jansen, R. C., Shi, Y., Chen, J., Hu, Y., Xu, C., Hong, S., Li, J., Zhang, M.: Using hourly measurements to explore the role of secondary inorganic aerosol in $PM_{2.5}$ during haze and fog in Hangzhou, China. Adv. Atmos. Sci., 31, 1427–1434, 2014.

Liu, M., Song, Y., Zhou, T., Xu, Z., Yan, C., Zheng, M., Wu, Z., Hu, M., Wu, Y., Zhu, T.: Fine particle pH during severe haze episodes in northern China. Geophys. Res. Lett., 44, 5213−5221, 2017.

Luo, X. S., Tang, A. H., Shi, K., Wu, L. H., Li, W. Q., Shi, W. Q., Shi, X. K., Erisman, J. W., Zhang, F., Liu, X. J.: Chinese coastal seas are facing heavy atmospheric nitrogen deposition. Environ. Res. Lett., 9, 095007, 2014.

Meng, C. C., Wang, L. T., Zhang, F. F., Wei, Z., Ma, S. M., Ma, J., Yang, J.: Characteristics of concentrations and water-soluble inorganic ions in $PM_{2.5}$ in Handan City, Hebei province, China. Atmos. Res., 171, 133−146, 2016.

Saraswati, Sharma, S. K., Saxena, M., Mandal, T. K.: Characteristics of gaseous and particulate ammonia and their role in the formation of secondary inorganic particulate matter at Delhi, India. Atmos. Res., 218, 34–49, 2019.

Shen, J., Liu, X., Ying, Z., Fangmeier, A., Goulding, K., Zhang, F.: Atmospheric ammonia and particulate ammonium from agricultural sources in the North China Plain. Atmos. Environ., 45, 5033–5041, 2011.

Song, S., Gao, M., Xu, W., Shao, J., Shi, G., Wang, S., Wang, Y., Sun, Y., Mcelroy, M. B.: Fine particle pH for Beijing winter haze as inferred from different thermodynamic equilibrium models. Atmos. Chem. Phy., 18, 7423−7438, 2018.

Stein, A.F., Draxler, R.R., Rolph, G.D., Stunder, B.J.B., Cohen, M.D. and Ngan, F.: NOAA's HYSPLIT atmospheric transport and dispersion modeling system. Bull. Am. Meteorol. Soc. 96: 2059–2077, 2015.

Tanner, P.A.: Vehicle-related ammonia emissions in Hong Kong. Environ. Chemi. Lett., 7, 37–40, 2009.

Tian, S., Pan, Y., and Wang, Y.: Ion balance and acidity of size-segregated particles during haze episodes in urban Beijing. Atmospheric Research 201, 159–167, 2018.

Walker, J. T., Whitall, D. R., Robarge, W. P., Paerl, H. W.: Ambient ammonia and ammonium aerosol across a region of variable ammonia emission density. Atmos. Environ., 38, 1235–1246, 2004.

Wang, C., Yin, S., Bai, L., Zhang, X., Gu, X., Zhang, H., Lu, Q., Zhang, R.: High-resolution ammonia emission inventories with comprehensive analysis and evaluation in Henan, China, 2006–2016. Atmos. Environ., 193, 11–23, 2018.

Wang, H., Yang, F., Shi, G., Tian, M., Zhang, L., Zhang, L., Fu, C.: Ambient concentration and dry deposition of major inorganic nitrogen species at two urban sites in Sichuan Basin, China. Environ. Pollut., 219, 235–244, 2016.

Wu, S., Dai, L., Wei, Y., Zhu, H., Zhang, Y., Schwab, J. J., Yuan, C.: Atmospheric ammonia measurements along the coastal lines of Southeastern China: Implications for inorganic nitrogen deposition to coastal waters. Atmos. Environ., 177, 1–11, 2018.

Zhang, R., Sun, X., Huang, Y., Shi, A., Yan, J., Nie, T., Yan, X., Li, X.: Secondary inorganic aerosols formation during haze episodes at an urban site in Beijing, China. Atmos. Environ., 177, 275–282, 2018.